# Quantifying the Entropic and Energetic Effects of Linker Length and Rigidity within Synthetic HIV-1 Antibodies designed to Bind Bivalently to Env Spikes

Rachel P. Galimidi[a,b,*], Tal Einav[c,*], Priyanthi N. P. Gnanapragasam[a], Devashish S. Joshi[a,d], Anne M. Lynch[a,e], Shahrzad Yazdi[f], Anthony P. West, Jr.[a], Rob Phillips[a,c,g,**], and Pamela J. Bjorkman[a,**]

[a]Division of Biology and Biological Engineering, California Institute of Technology, Pasadena, CA 91125

[b]Present address: Canary Center at Stanford, Department of Radiology, Stanford University School of Medicine, Stanford, CA, USA.

[c]Department of Physics, California Institute of Technology, Pasadena, CA 91125

[d]Present address: Medical College of Wisconsin, Milwaukee, WI, 53226, USA

[e]Present address: Program in Developmental Biology, Baylor College of Medicine, 1 Baylor Plaza, Houston, Tx 77030

[f]Department of Materials Science and Engineering, Massachusetts Institute of Technology, Cambridge, MA, 02139, USA

[g]Department of Applied Physics, California Institute of Technology, Pasadena, CA 91125

* These authors contributed equally
** Co-corresponding authors

## Abstract

Due to the low density of envelope (Env) spikes on the surface of HIV-1, neutralizing IgG antibodies rarely bind bivalently using both antigen-binding arms (Fabs) to crosslink between spikes, instead resorting to weaker monovalent binding that is more sensitive to Env mutations. Synthetic antibodies capable of bivalently binding within single Env trimers (intra-spike crosslinking) were previously shown to exhibit increased neutralization potencies. In initial work, diFabs joined by varying lengths of rigid double-stranded DNA (dsDNA) were considered. Here we investigated whether linkers with different rigidities could enhance diFab potency by synthesizing DNA-Fabs containing different combinations of rigid dsDNA and flexible single-stranded DNA (ssDNA) and created a model that predicts their neutralization potencies. Model predictions, verified by experimental data, show that although a long flexible polymer may be capable of bivalent binding, it exhibits weak neutralization due to the large loss in entropic degrees of freedom during bivalent binding. In contrast, the strongest neutralization potencies require a rigid linker that optimally spans the distance between two Fab binding sites on an Env trimer. These results inform the design of bivalent anti-HIV-1 therapeutics that utilize avidity effects to remain potent against HIV-1 in the face of the rapid mutation of Env spikes.

## Significance

Effective antibody-mediated immune responses against pathogens involve tight binding to invading particles. IgG antibodies usually accomplish this by simultaneously binding two antigen-binding arms (Fabs) to a dense array of antigens on the pathogen – if one Fab dissociates, IgGs can remain attached through the second arm, enhancing the likelihood that the first Fab will reassociate. This avidity effect enables bivalent IgGs to achieve a higher apparent affinity for the pathogen than a monovalent Fab. HIV-1 foils this strategy by having few, highly-separated Envelope spikes (Envs) on its surface for IgGs to bind. This forces most anti-HIV-1 antibodies to bind monovalently, causing IgGs to rapidly dissociate from mutated strains of HIV-1 that arise during infection. In this work, we explore the efficacies of an array of synthetic antibodies that achieve avidity through bivalent binding to single trimeric Envs. We develop a model that uses the geometry of each synthetic antibody to predict its neutralization potency, quantifying how entropic effects determine neutralization potencies and presenting a way to theoretically design an optimal antibody-based reagent that can bind bivalently to HIV-1 Env in order to target the virus in the face of its rapid mutation.

## Introduction

Despite decades of research since its discovery, Human Immunodeficiency Virus-1 (HIV-1) continues to threaten global public health (1). While there have been advances in our understanding of the mechanisms of infection and the development of preventative and therapeutic strategies, there remains no cure for HIV-1 infection. Antiretroviral therapy with small molecule drugs can control the progression of the virus, allowing those infected with HIV-1 to live longer and healthier lives, but the treatment includes detrimental side effects, and when discontinued or not taken as prescribed, leads to viral rebound to pre-treatment levels (2). A major factor confounding the development of a prophylactic vaccine is the rapid mutation of HIV-1, leading to the emergence of many new strains, even within a single individual (3). Thus most antibodies raised by the host immune system are strain-specific or neutralize only a subset of strains, leading to viral escape from host antibodies.

Recent interest has focused upon the isolation of broadly neutralizing IgG antibodies (bNAbs) from a subset of HIV-1–infected individuals (4). These antibodies bind to and block the functions of the HIV-1 envelope (Env) spike, the viral protein responsible for fusion of the HIV-1 and target cell membranes that leads to entry of the virion's genetic material into the host cell (5). The discovery and characterization of HIV-1 bNAbs has brought new impetus to the idea of passively delivering antibodies to protect against or treat HIV-1 infection. bNAbs can prevent and treat infection in animal models (6-12) and exhibited efficacy against HIV-1 in human trials (13-16). However, HIV-1 Env mutates to become resistant to any single bNAb, as evidenced by the fact that NAbs developed in an infected individual, even NAbs that can neutralize large numbers of viral variants in laboratory assays, normally fail to neutralize autologous circulating viral strains (17-20). As a result, antibodies that develop during HIV-1 infection appear to be unable to control the virus in an infected individual.

We previously proposed that one mechanism by which HIV-1 evades antibodies more successfully than other viruses arises from the low surface density of Env spikes that can be targeted by neutralizing antibodies (21, 22). Compared to viruses such as influenza A, dengue, and hepatitis B, the density of Env spikes on the surface of HIV-1 is about two orders of magnitude smaller (22). For example, influenza A has ≈450 spikes per virion, whereas each HIV-1 virion incorporates only 7-30 Env spikes (average of 14) (22-26), even though both are enveloped viruses with ≈120 nm diameters (Fig. 1A). The HIV-1 spikes are the machinery by which the virus binds its host receptor CD4 and coreceptor CCR5/CXCR4 to mediate the fusion of the host and viral membranes that allows its genome to enter target cells (5). As a consequence of its small number of spikes, HIV-1 infection of target cells is inefficient; the transmission probabilities for sexually-acquired HIV-1 infection range from 0.4 to 1.4% (27). However, the reduced infectivity of HIV-1 comes with a concomitant reduction in the ability of antibodies to control the virus, as the surface spikes serve as the only targets for neutralizing antibodies that can block infection of target cells (4).

The close spacing of spikes on typical viruses allows IgG antibodies to bind bivalently to neighboring spikes (inter-spike crosslinking) using both of their antigen-binding arms (Fabs). However, most spikes on HIV-1 virions are too far apart to permit inter-spike crosslinking by IgGs, whose antigen-binding sites are separated by ≤15 nm (28). While each homotrimeric HIV-1 spike includes three binding sites (epitopes) for an antibody, the architecture of HIV-1 Envs and distribution of epitopes on the HIV-1 Env trimer prohibits simultaneous binding of two Fabs within a single IgG (intra-spike crosslinking) to the same Env (29, 30). We suggested that predominantly monovalent binding by anti-HIV-1 antibodies expands the range of Env mutations

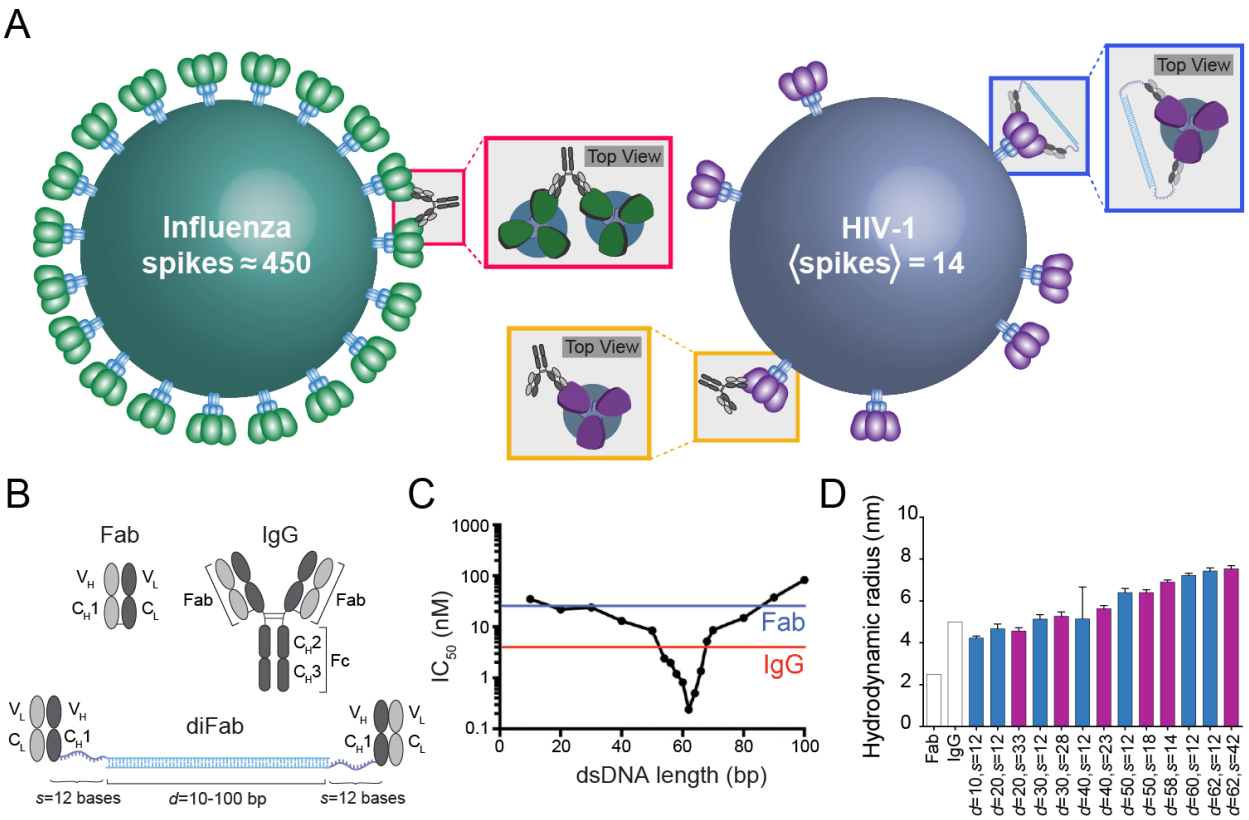


**Fig. 1. Effects of spike density on IgG binding.** (A) Close spacing of hundreds of surface spikes on influenza A allows bivalent binding of IgGs to adjacent spikes (red boxes), permitting avidity effects in the context of low monovalent (i.e., Fab-antigen) affinities. In contrast, HIV-1 has an average of 14 spikes that are spaced far apart, and because the HIV-1 spike architecture prohibits simultaneous binding of two Fabs to a single Env trimer, most IgGs bind monvalently to HIV-1 Envs (gold boxes). We investigated a synthetic homo-diFab designed to bind bivalently to a single HIV-1 spike trimer (blue boxes). (B) Schematics of a Fab, an IgG, and a diFab composed of two Fabs joined by a ssDNA and dsDNA linker of length *d* bp flanked on both sides by *s*=12 bases of ssDNA. (C) Comparison of $IC_{50}$ values from in vitro neutralization assays measuring the potencies of 3BNC60 diFabs with *d* = 10 to *d* = 100 bp dsDNA and *s* = 12 bases for neutralizing HIV-1 strain 6535.3 (data from (21)). The $IC_{50}$ values from (21) for 3BNC60 Fab and 3BNC60 IgG against HIV-1 strain 6535.3 are shown as blue (Fab) and red (IgG) lines. (D) Comparison of hydrodynamic radii of diFabs constructed using linkers containing the indicated numbers of dsDNA bps (*d*) and ssDNA bases (*s*). Blue bars represent previously-constructed diFabs (Panel C; Table 1) (21); purple bars denote new diFabs with longer ssDNA (Table 2). Mean values are plotted with error bars for standard deviations of measurements made in triplicate.

permitting antibody evasion, whereas reagents capable of bivalent binding through inter- or intra-spike crosslinking would be more resistant to Env mutations and thus more potent across multiple strains of HIV-1 (21, 22). The hypothesis that HIV's low spike numbers and low densities contributes to the vulnerability of HIV-1 bNAbs to spike mutations is supported by independent biochemical and EM studies demonstrating that HIV-1 has an unusually low number of spikes that are not clustered (23-26, 31), and that bivalent IgG forms of anti-HIV-1 NAbs are only modestly more effective than monovalent Fabs, by contrast to bivalent IgGs against other viruses, which can be 100s- to 1000s-fold more potent than counterpart monovalent Fabs (21, 22, 29, 30).

An antibody's neutralization potency against a virus is related to its antigen-binding affinity, which is defined as the binding strength between a Fab and its antigen (32) described by the equilibrium dissociation constant $K_D$ = [Fab][Ag]/[Fab–Ag], where [Fab], [Ag] and [Fab–Ag] are the concentrations of the antibody Fab, antigen, and the complex, respectively (33). In bivalent molecules interacting with binding partners that are tethered to a surface, the apparent affinity, or avidity, can be enhanced by multivalent binding. Such multivalent interactions are seen in many biological contexts including cell-cell communication, virus-host cell interactions, antibody-antigen interactions, and Fc receptor interactions with antigen-antibody complexes (34). Avidity effects benefit these interactions from both kinetic and thermodynamic standpoints: binding bivalently to tethered binding partners is advantageous kinetically because if one arm dissociates, the likelihood of it finding its binding partner is greater due to the constraint of being tethered (35). Avidity effects are also advantageous thermodynamically; whereas binding the first arm results in losses of translational and rotational degrees of freedom, the subsequent binding of the second arm incurs a smaller entropic cost, thereby increasing the likelihood of the bivalent state (35).

In the context of an IgG with two antigen-binding Fabs, the ability to bind bivalently is dependent on geometric factors such as the separation distances and orientations of tethered epitopes (36). In the case of IgG-virus interactions, the tethered epitopes would be on adjacent spikes during inter-spike crosslinking or on individual spikes if intra-spike crosslinking can occur. Although the architecture of the HIV-1 spike prevents intra-spike crosslinking (29, 30), we engineered reagents (homo- and hetero-diFabs) that can simultaneously bind to a single spike trimer, resulting in mean neutralization potency increases >100-fold over a panel of HIV-1 strains (21). Our intra-spike crosslinking reagents were IgG Fabs joined by different lengths of double-stranded DNA (dsDNA), which served as both a rigid linker and a molecular ruler to probe the conformations of HIV-1 Env on virions (21) (Fig. 1B). Optimal diFabs inhibited HIV-1 infection of reporter target cells more efficiently than the parental IgG or Fab (Fig. 1C; data shown from (21) for neutralization of HIV-1 strain 6535.3 by a homo-diFab constructed from 3BNC60, a CD4-binding site bNAb (37), linked by varying lengths of dsDNA). This response showed a sharp dependence on the length of the dsDNA linker between the two Fabs (Fig. 1C), suggesting that dsDNA can be used as a ruler to measure the approximate distance between epitope binding sites on virion Envs and to design reagents capable of strong intra-spike crosslinking between such sites. The large potency increases observed for diFabs with optimal dsDNA linkers supports the hypothesis that low spike densities facilitate antibody evasion by HIV-1 (21).

While these results suggested that a rigid, optimal-length linker joining two HIV-1 bNAb Fabs could result in synergistic binding and neutralization of HIV-1 through avidity effects, they did not rule out the possibility that a flexible linker joining two Fabs could also enhance potency. For example, if maximal potency in an intra-spike crosslinking diFab does not require a rigid linker spanning the precise distance between epitopes on trimeric HIV-1 Env, it should be possible to create IgGs that bind with avidity to any Env epitope using a protein-based flexible linker. A more flexible linker could potentially improve the antigen-binding orientation and hence affinity of the Fab, but it would also increase the entropic penalty associated with bivalent binding (35). To investigate which effect was dominant, flexible $Gly_4Ser$ repeats were introduced into the hinge regions of IgGs to extend their reach, but the resulting constructs did not show increased potencies (38).

In this work, we created 11 new diFabs with DNA linkers to systematically evaluate the effects of linker rigidity on synergistic neutralization by a diFab constructed from the CD4-binding site bNAb 3BNC60. Starting with (*d*=62, *s*=12) (two 3BNC60 Fabs joined by a 62 bp (base pair) dsDNA linker flanked by 12 bases of ssDNA on both ends (21)), we considered new linker

designs in order to characterize the roles of rigidity and flexibility versus overall length of DNA linker within a series of 3BNC60 diFabs. Using in vitro neutralization assays, we found that substituting flexible ssDNA for rigid dsDNA in the linker reduced neutralization potency. To quantify this effect, we created a statistical mechanics-based mathematical model that characterized the various synthetic antibodies we created, demonstrating that the efficacy of intra-spike crosslinking/increased neutralization potency could be explained solely by entropic effects. Using this model, we can predict the neutralization potential of other synthetic bivalent antibodies and of more complicated geometries involving additional Fabs. Insights from our synthetic constructs can be adapted to antibody design in other systems in which length and rigidity of linkers in multivalent reagents must be balanced to elicit the most effective response.

## Results

### Experimental results establish parameters for modeling

Before describing the new diFab designs, we summarize previous results from which we derived model parameters used in this work. To evaluate our hypothesis that anti-HIV-1 reagents that bind bivalently would be more potent across multiple strains of HIV-1 (22), we engineered antibody-based molecules to bind bivalently through intra-spike crosslinking (21). We first made a library of bNAb Fabs, covalently attached them to ssDNA, and then hybridized the ssDNA to different lengths of dsDNA to make diFabs connected by different lengths of dsDNA (Fig. 1B). The dsDNA served as a molecular ruler by virtue of its long persistence length (dsDNA is essentially rigid up to ≈150 bp) and its 0.34 nm/bp increment (39). We then assayed diFabs against a panel of HIV-1 strains to identify optimal distances for increased breadth and potency compared to their parental Fabs and IgGs.

We determined the optimal dsDNA linker length for the 3BNC60 diFab by evaluating dsDNA linkers using in vitro neutralization assays in which different concentrations of a synthetic antibody were evaluated for their ability to prevent HIV-1 infection of target cells (40). We found that the 50% inhibitory concentrations ($IC_{50}$ values) of 3BNC60 diFabs against HIV-1 strain 6535.3 were sharply dependent on the dsDNA length, with the most potent 3BNC60 diFab containing 62 bp of dsDNA with 12 bases of flanking ssDNA on both sides of the linker (Fig. 1C). This diFab, here called (*d*=62, *s*=12), exhibited synergistic neutralization (up to 167-fold increased potency with respect to individual HIV-1 strains and a 19-fold average increase across a virus panel), which we hypothesized resulted from avidity effects due to intra-spike crosslinking in which the diFab bound to two of its three adjacent epitopes on a single HIV-1 Env trimer (21).

The length of the double-stranded region of this optimal linker (21 nm) was close to the predicted distance (≈20 nm) between the C-termini of adjacent 3BNC60 Fabs (where the DNA was covalently attached) bound to a low-resolution open structure of an HIV-1 trimer (41). Bridge lengths of ≈60 bp of dsDNA also exhibited the best potencies for 3BNC60 diFabs and related CD4-binding site diFabs against other HIV-1 strains, although the neutralization potency increases for diFabs containing ≈60 bp of dsDNA were not as pronounced as the 3BNC60 homo-diFabs assayed against the 6535.3 HIV-1 strain (21). We therefore chose the neutralization data for the (*d*=62, *s*=12) diFab against the 6535.3 HIV-1 strain for modeling (Fig. 1C; Table 1).

To model the linkers connecting the two Fabs in our synthetic antibodies, we treated the dsDNA as a 1D rigid rod and the ssDNA as a random walk. The former assumption is valid because the linkers in all constructs include ≤100 bp of dsDNA, less than its 150 bp persistence length (42).

Free ssDNA is flexible with a persistence length between 2-6 bases (43, 44), and because each of our constructs consist of ssDNA segments with at least 12 bases, we analyzed the ssDNA as a floppy chain using polymer physics models (e.g., the ideal chain model, the worm-like chain model) (45).

To experimentally assess the degree to which the flanking ssDNA affects the Fab separation in diFabs, we used dynamic light scattering (DLS) (46) to measure the hydrodynamic radii of our diFabs. We previously used DLS to show that diFabs with a fixed amount of ssDNA (12 bases) and variable numbers of dsDNA bps exhibited increasing radii as dsDNA linker length (21), consistent with the assumption that the dsDNA in diFab linkers behaves as a rigid rod. Here we used DLS to compare the effects of different numbers of ssDNA bases flanking a dsDNA bridging linker (Fig. 1D, where blue bars represent diFabs from Fig 1C (Table 1) and purple bars denote new diFabs with longer flanking ssDNA segments (Table 2)). The hydrodynamic radii of diFabs did not depend on the length of the ssDNA; e.g., the (*d*=62, *s*=12) diFab had the same hydrodynamic radius as (*d*=62, *s*=42). These results suggest that the ssDNA in the linker does not behave as an ideal free polymer, but rather that its extension is more limited within the diFab experimental system.

Because the DLS data suggested that the effective length of ssDNA in our system is more confined than for free ssDNA, the contribution of the ssDNA was determined empirically by comparing the diFab neutralization data to two models for ssDNA: (1) a model in which the ssDNA in the diFab linker was completely ignored by assuming it has zero length (Fig. 2A), and (2) a model in which the ssDNA contributed to the linker but with a smaller persistence length than when free in solution (Fig. 2B).

One further model parameter, $l_{\mathrm{flex}}$, was included to account for variations in the distance between the C-termini of the two 3BNC60 $C_H1$ domains to which the DNA was attached due to the following factors: (*i*) The Fab $C_H1$-$C_L$ domains can adopt different conformations with respect to $V_H$-$V_L$ (47) such that the locations of the $C_H1$ C-terminus could shift by up to ≈1 nm, (*ii*) Residues C-terminal to $C_H1$ residue 217 are disordered in the 3BNC60 Fab structure (37), thus the position of the $C_H1$ residue to which the DNA was attached (Cys233) is uncertain within ≈1 nm, (*iii*) The ssDNA is covalently linked to the $C_H1$ residue Cys233 using an amine-to-sulfhydryl crosslinker (Sulfo-SMCC) (Methods), which exerts unknown effects on the length and the degree of flexibility between the ssDNA and Fab.

**Relating Antibody Neutralization to the Probability that an HIV-1 Spike is Bound**

We next created a mathematical model of diFab efficacy based on the properties of the linker. To lay the groundwork for this model, we first related the ability of a diFab to neutralize an HIV-1 virion to the probability that an Env spike on the surface of HIV-1 will be bound. Each Env spike is a homotrimer with three identical binding sites for a 3BNC60 Fab (48). The spikes are assumed to be sufficiently far apart that a diFab cannot crosslink between neighboring spikes. A diFab with the right geometry can bind to two binding sites on the same spike, whereas a diFab whose linker is either too short or too long can bind to only a single Env epitope ( Fig. A). Previous experiments suggested that only one of the three CD4 binding sites on an Env spike need to be bound to prevent the Env from functioning in membrane fusion (49). We imposed a soft threshold for virus entry where the ability of an HIV-1 virion to infect increases linearly from zero (when all spikes are bound by diFabs) to some maximum value (when all spikes are unbound) that is constant across all HIV-1 molecules (Appendix A). While some studies suggested that two or three Env trimers are required for HIV-1 to infect (50, 51), other studies found that only one functional Env trimer was required for target cell fusion (52); thus

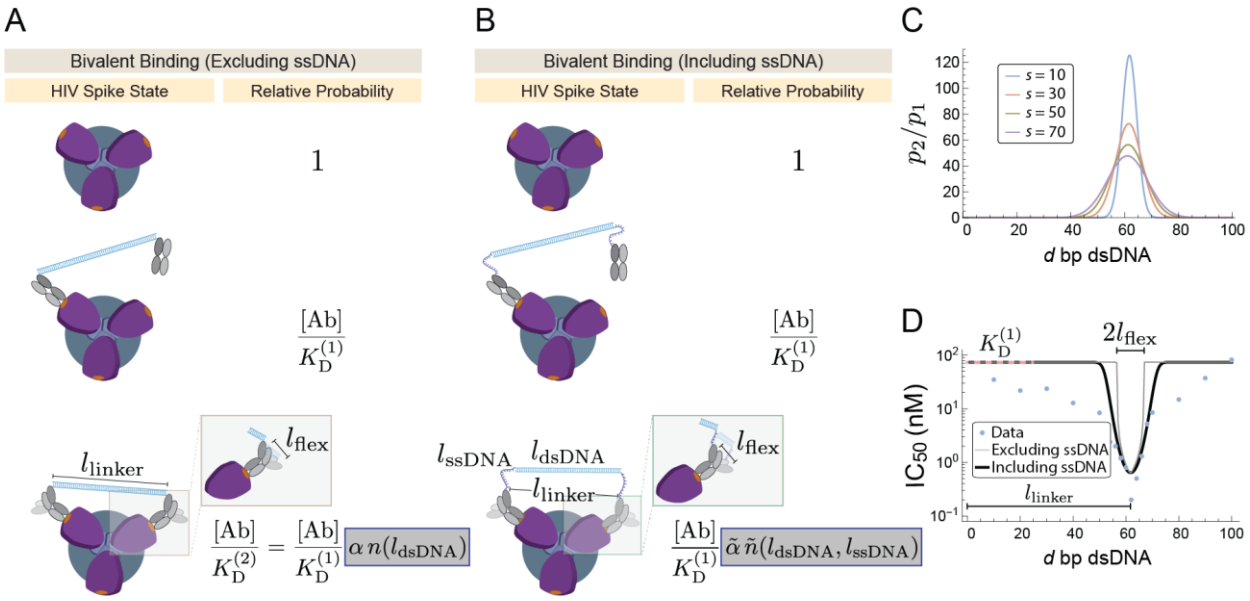


**Fig. 2. Modeling the optimal linker length for a diFab.** (A) DLS data suggested that the diFab linker can be modeled by either (A) ignoring the ssDNA entirely or (B) including the ssDNA with a smaller persistence length. In both models, the Boltzmann weight of the monovalent state is dictated by the $K_D^{(1)}$ (the dissociation constant between the Env trimer and the first diFab arm), while the weight of the bivalent state is dictated by a geometric or avidity factor ($\alpha n$ in Panel A and $\tilde{\alpha}\tilde{n}$ in Panel B) shown in a gray box. This geometric factor depends upon the length of the dsDNA and ssDNA in each construct as well as on the optimal length $l_{\text{linker}}$ of the linker between two bound Fabs and the flexibility $l_{\text{flex}}$ between the $C_H1$-$C_L$ and $V_H$-$V_L$ domains of a bound Fab. The ability to neutralize is given by the sum of the probabilities of the monovalent and bivalent states. (C) The relative probability that a diFab with d bp dsDNA and s bases ssDNA in its linker is bivalently ($p_2$) versus monovalently ($p_1$) bound. (D) Comparison of experimental (points) and predicted (curves) effects of dsDNA bridge lengths on the neutralization potencies of the 3BNC60 diFabs against HIV-1 strain 6535.3 (data from (21)). Experimental neutralization $IC_{50}$s showed a sharp dependence on dsDNA linker length, with an optimum length at *d*=62 bp. Parameters for both models were inferred by nonlinear fitting (see Methods).

our model allowed a virion with a single unbound Env trimer to infect, albeit $1/n$ as effectively as a virion with $n$ unbound trimers.

Given these assumptions, the ability of a diFab to neutralize HIV-1 is proportional to the probability that at least one of the CD4 binding sites of an HIV-1 spike will be bound by a 3BNC60 Fab (Appendix A). For example, if each Env protein has a 75% chance to be bound by a diFab, an average of 75% of the spikes on each virion will be bound, and by the linearity assumption, the HIV virions will be 75% neutralized. This enables us to relate the experimentally-determined % neutralization for diFabs in Tables 1 and 2 to the theoretically-tractable probability that a single Env spike will be bound either monovalently or divalently by a diFab. Avidity effects will allow an optimal diFab to bind more tightly (with a lower apparent $K_D$) to a spike, increasing the binding probability and the neutralization potency.

### The Avidity of a diFab is Constrained by the Length of Rigid dsDNA and Essentially Independent of Flanking Flexible ssDNA

To calculate the probability that any of the 3BNC60 binding sites on an HIV-1 spike are occupied, we enumerated three potential states of the spike, which represent a single diFab bound to zero, one, or two adjacent binding sites. Because measurements of the hydrodynamic

radii of multiple constructs suggested that the ssDNA components of the linker did not measurably alter its size, we first modeled the system as a pair of Fabs joined together with dsDNA and ignored the contributions of the ssDNA (Fig. 2A).

When a diFab transitions from the unbound state (with probability $p_0$) to a monovalently-bound state (with probability $p_1$), it loses translational and rotational entropy but gains favorable binding energy (53) leading to the relative probability

$$\frac{p_1}{p_0} = \frac{[\mathrm{Ab}]}{K_{\mathrm{D}}^{(1)}}, \qquad [1]$$

where $K_{\mathrm{D}}^{(1)}$ is the equilibrium dissociation constant of the first diFab arm binding to Env. Note that $K_{\mathrm{D}}^{(1)}$ incorporates the geometry of the Env trimer, namely, that there are three 3BNC60 binding sites on a trimeric HIV-1 spike and that the diFab can bind monovalently with either arm. Importantly, the transition from an unbound to a monovalently-bound diFab is independent of the composition of the diFab's linker, since the loss in translational and rotational entropy increases slowly with the size of a particle and hence can be assumed to be the same for all constructs. This implies that the constant $K_{\mathrm{D}}^{(1)}$ will be the same for all diFabs in this study and that it also characterizes the 3BNC60 Fab's binding to the Env trimer. By assuming that the neutralization potency of the Fab is proportional to how well it binds to the HIV-1 spike, the value of $K_{\mathrm{D}}^{(1)}$ is given by the Fab $IC_{50} = 74 \pm 31$ nM (see Methods), a value consistent with experimental $K_D$ values reported for binding of a Fab from a CD4-binding site bNAb to a soluble, trimeric form of HIV-1 Env (54). In viral contexts in which the relationship between the apparent $K_D$ of an antibody and its $IC_{50}$ is more complex, the dissociation constant could instead be inferred by nonlinear fitting.

We now turn to the transition from a monovalently-bound diFab to a bivalently-bound diFab. The ability to bivalently bind strongly depends on the size of the diFab's linker, since having too large or too small a linker will preclude bivalent binding through intra-spike crosslinking. The relative probability of each energy state is proportional to its Boltzmann weight, $e^{-\beta(E-TS)} = \Omega\, e^{-\beta E}$, where $\beta = \frac{1}{k_B T}$, $E$ is the energy, $T$ is the temperature (37˚C), $k_B$ represents Boltzmann's constant, $S = k_B \log \Omega$ is the entropy, and $\Omega$ is the number of microstates with a given energy. Thus, the relative probabilities of the bivalent and monovalent states satisfy

$$\frac{p_2}{p_1} = \frac{\Omega_2}{\Omega_1} e^{-\beta(E_2 - E_1)} \qquad [2]$$

where $p_j$, $E_j$, and $\Omega_j$ represent the probability, energy, number of microstates when $j$ Fabs are bound to an Env.

The number of configurations $\Omega_1$ for a monovalently-bound diFab is proportional to the degrees of freedom available when one Fab is bound to its epitope and the second Fab is unbound and tethered to the first by DNA. Since the associated entropy of this motion increases slowly with size, we assume that $\Omega_1$ is constant across all diFabs. Similarly, the binding energy $E_2 - E_1$ gained when the second Fab in a diFab binds to the HIV-1 spike is the same for all diFabs we consider.

The number of configurations $\Omega_2$ of the bivalent state depend upon the entropy of the dsDNA linker joining the C-termini of the two bound Fabs separated by a width $l_{\mathrm{linker}}$ (Fig. 2A). In addition, each Fab is inherently flexible at the join between the $C_H1$-$C_L$ domains and the $V_H$-$V_L$ domains, as denoted by $l_{\mathrm{flex}}$. If we approximate $l_{\mathrm{linker}}$ and $l_{\mathrm{flex}}$ as colinear so that the problem becomes one dimensional (see Appendix B), the number of microstates corresponding to the bivalently-bound state satisfies

$$\Omega_2 = \frac{\max(l_{\mathrm{flex}} - |l_{\mathrm{dsDNA}} - l_{\mathrm{linker}}|, 0)}{\Delta l} \equiv \frac{n(l_{\mathrm{dsDNA}})}{\Delta l} \quad [3]$$

where $n(l_{\mathrm{dsDNA}})$ equals the length between the outer-most dsDNA orientations capable of bivalent binding (Appendix B Fig. S2), and $\Delta l$ is a constant representing the discretization of this length so that $\Omega_2$ is unitless. In short, $n(l_{\mathrm{dsDNA}})$ quantifies how the geometry of the diFab affects its ability to bivalently bind to a spike.

Using Eqs. 1-3 and the normalization condition, $p_0 + p_1 + p_2 = 1$, the probability that at least one of the three Fab epitopes on an HIV-1 spike will be bound can be written as

$$p_1 + p_2 = \frac{\frac{[\mathrm{Ab}]}{K_{\mathrm{D}}^{(1)}} + \frac{[\mathrm{Ab}]}{K_{\mathrm{D}}^{(1)}} \alpha\, n(l_{\mathrm{dsDNA}})}{1 + \frac{[\mathrm{Ab}]}{K_{\mathrm{D}}^{(1)}} + \frac{[\mathrm{Ab}]}{K_{\mathrm{D}}^{(1)}} \alpha\, n(l_{\mathrm{dsDNA}})} \quad [4]$$

where we have separated the constant $\alpha = \frac{1}{\Omega_1 \Delta l} e^{-\beta(E_2 - E_1)}$, which does not depend on the diFab geometry, from $n(l_{\mathrm{dsDNA}})$, which does. Because $p_1 + p_2$ is proportional to the % neutralization of the HIV virion, the $\mathrm{IC}_{50}$ of each diFab with the contribution of the ssDNA excluded is given by

$$\mathrm{IC}_{50}^{\text{exc ssDNA}} = \frac{K_{\mathrm{D}}^{(1)}}{1 + \alpha\, n(l_{\mathrm{dsDNA}})}. \quad [5]$$

Nonlinear fitting the $IC_{50}$ values of all diFab constructs in Tables 1 and 2 led to the dissociation constant $K_D^{(1)} = 74$ nM characterizing the first diFab arm binding to Env, the optimal linker length $l_{\mathrm{linker}} = 21$ nm between bound Fabs, the flexibility $l_{\mathrm{flex}} = 1.8$ nm between the Fab $C_H1$-$C_L$ and $V_H$-$V_L$ domains, and the avidity constant $\alpha = 70$ (see Methods). Fig. 2D (gray line) shows the model predictions which roughly approximate the shape of the $IC_{50}$ values. diFabs that are too long or too short cannot bivalently bind, leading to a sharp transition in the $IC_{50}$ for dsDNA shorter than $l_{\mathrm{linker}} - l_{\mathrm{flex}} = 19.2$ nm (57 bp) or longer than $l_{\mathrm{linker}} + l_{\mathrm{flex}} = 22.8$ nm (69 bp). We hypothesized that including the ssDNA in the model would smooth the transition from the bivalent to purely monovalent binding, and next explored how the effects of the ssDNA in the linker could be modeled.

With contributions of ssDNA included, the distance $l_{\mathrm{linker}}$ between the C-termini of bivalently bound Fabs must be spanned by the rigid dsDNA segments as well as the two flanking ssDNA strands (Fig. 2B). We modeled each ssDNA segment as a random walk using an ideal chain model with a persistence length of $\xi_{\mathrm{ssDNA}} = 0.1$ nm inferred by nonlinear fitting (see Methods). Note that this persistence length is smaller than the length of a ssDNA base (0.63 nm) to account for the DLS data showing no effects on measured hydrodynamic radii of diFabs with linkers containing different amounts of ssDNA (Fig. 1D).

Of the multiple configurations that two ssDNA random walks can take on, only a small fraction will end at the proper distance $l_{\mathrm{linker}}$ to allow a diFab to bivalently bind. The probability density that the linker will obtain one of these limited configurations can be computed analytically (Appendix C) as

$$p(l_{\mathrm{dsDNA}}, l_{\mathrm{ssDNA}}, l_{\mathrm{linker}}) = \frac{1}{l_{\mathrm{linker}}\, l_{\mathrm{dsDNA}}} \sqrt{\frac{3}{32\pi^3 l_{\mathrm{ssDNA}} \xi_{\mathrm{ssDNA}}}}\, e^{-\frac{3\left(l_{\mathrm{linker}}^2 + l_{\mathrm{dsDNA}}^2\right)}{8 l_{\mathrm{ssDNA}} \xi_{\mathrm{ssDNA}}}} \sinh\left(\frac{3\, l_{\mathrm{linker}}\, l_{\mathrm{dsDNA}}}{4\, l_{\mathrm{ssDNA}} \xi_{\mathrm{ssDNA}}}\right), \quad [6]$$

where $l_{\mathrm{dsDNA}} = d\left(0.34 \frac{\mathrm{nm}}{\mathrm{bp}}\right)$ and $l_{\mathrm{ssDNA}} = s\left(0.64 \frac{\mathrm{nm}}{\mathrm{base}}\right)$ represent the length of dsDNA and ssDNA segments in the linker, respectively. Analogously to Eq. 3, the flexibility of the Fab implies that the dsDNA and ssDNA can span any length from $l_{\mathrm{linker}} - l_{\mathrm{flex}}$ to $l_{\mathrm{linker}} + l_{\mathrm{flex}}$ (see Appendix C). In the limit where $1\ \mathrm{nm} \approx l_{\mathrm{flex}} \ll l_{\mathrm{linker}} \approx 20\ \mathrm{nm}$, the number of bivalent configurations is proportional to the simple form

$$\tilde{n}(l_{\mathrm{dsDNA}}, l_{\mathrm{ssDNA}}) = l_{\mathrm{flex}}^2\, p(l_{\mathrm{dsDNA}}, l_{\mathrm{ssDNA}}, l_{\mathrm{linker}}). \quad [7]$$

As in the model neglecting ssDNA described in the previous section, all other constants that are independent of the diFab geometry can be absorbed into a prefactor $\tilde{\alpha}$ in the bivalent state (Fig. 2B). Thus, the occupancy probability for an HIV-1 spike is given by the same functional form as Eq. 4, namely,

$$p_1 + p_2 = \frac{\frac{[\mathrm{Ab}]}{K_{\mathrm{D}}^{(1)}} + \frac{[\mathrm{Ab}]}{K_{\mathrm{D}}^{(1)}}\, \tilde{\alpha}\, \tilde{n}(l_{\mathrm{dsDNA}}, l_{\mathrm{ssDNA}})}{1 + \frac{[\mathrm{Ab}]}{K_{\mathrm{D}}^{(1)}} + \frac{[\mathrm{Ab}]}{K_{\mathrm{D}}^{(1)}}\, \tilde{\alpha}\, \tilde{n}(l_{\mathrm{dsDNA}}, l_{\mathrm{ssDNA}})} \quad [8]$$

with an analogous $\mathrm{IC}_{50}$ given by

$$\mathrm{IC}_{50}^{\mathrm{inc\ ssDNA}} = \frac{K_{\mathrm{D}}^{(1)}}{1 + \tilde{\alpha}\, \tilde{n}(l_{\mathrm{dsDNA}}, l_{\mathrm{ssDNA}})}. \quad [9]$$

Nonlinear fitting Eq. 9 to the $\mathrm{IC}_{50}$s in Tables 1 and 2 led to the parameter values $K_D^{(1)} = 74$ nM, $l_{\mathrm{linker}} = 21\ \mathrm{nm}$, $l_{\mathrm{flex}} = 1.8\ \mathrm{nm}$, $\tilde{\alpha} = 5.2 \times 10^5$, and the ssDNA persistence length $\xi_{\mathrm{ssDNA}} = 0.1$ (see Methods and Appendix D). The avidity parameter $\tilde{\alpha}$ is orders of magnitude larger than the corresponding parameter ($\alpha = 70$) in the model neglecting ssDNA because the probability that the 3D random walk encompassed within $\tilde{n}(l_{\mathrm{dsDNA}}, l_{\mathrm{ssDNA}})$ will end at the particular distance to enable bivalent binding is small, thereby requiring a correspondingly larger avidity parameter.

Fig. 2C plots the probability that a diFab will be bivalently bound ($p_2$) relative to the monovalently bound probability ($p_1$) as the amount of dsDNA (*d*) and ssDNA (*s*) in the linker varies. The model captures the trend that bivalent binding is most likely when $l_{\mathrm{linker}} \approx l_{\mathrm{dsDNA}}$ around *d*=62 bp dsDNA, with the peak shifting very slightly leftwards as the amount of ssDNA increases, demonstrating how the root-mean-squared length of the ssDNA slowly increases. The black curve in Fig. 2D shows how the model incorporating ssDNA (Eq. 9) provides a broader transition of the bivalent to monovalent binding more in line with the published diFab data (21). Hence, we restrict the following analysis to this latter model that includes the contributions from both ssDNA and dsDNA within the linker.

**The diFab Model Allows Bivalent Binding Only when the dsDNA Length is Approximately Equal to the Length of the Linker it Spans**

To gain a qualitative understanding of the model including ssDNA (Eq. 9), we examined it in two limits: near the optimal geometry $l_{\mathrm{dsDNA}} \approx l_{\mathrm{linker}}$ where the ability to bind bivalently is maximum, and far from the optimal limit when the diFab is too short or too long to permit bivalent binding

through intra-spike crosslinking. Note that all these statements also hold for the model excluding ssDNA (Eq. 5) provided $\tilde{\alpha} \to \alpha$ and $\tilde{n} \to n$.

Near the optimal limit, corresponding to $l_{\mathrm{dsDNA}} \approx l_{\mathrm{linker}}$ or $d \approx 62$ bp, HIV-1 neutralization will occur predominantly from the bivalently-bound configuration rather than the monovalent state, $\frac{p_2}{p_1} = \tilde{\alpha}\,\tilde{n}(l_{\mathrm{dsDNA}}, l_{\mathrm{ssDNA}}) \gg 1$. Hence, the system is well approximated with each spike either being unbound or bivalently-bound such that

$$\mathrm{IC}_{50} \approx \frac{K_{\mathrm{D}}^{(1)}}{\tilde{\alpha}\,\tilde{n}(l_{\mathrm{dsDNA}}, l_{\mathrm{ssDNA}})}, \quad (\text{near optimal geometry}) \qquad [10]$$

corresponding to the trough in the black curve in Fig. 2D. If the potency of diFab 1 is $\mathrm{IC}_{50}^{(1)}$, and the potency of diFab 2 with a different linker is $\mathrm{IC}_{50}^{(2)}$, the latter diFab's potency will be shifted relative to the former by

$$\frac{\mathrm{IC}_{50}^{(2)}}{\mathrm{IC}_{50}^{(1)}} = \frac{\tilde{n}\left(l_{\mathrm{dsDNA}}^{(1)}, l_{\mathrm{ssDNA}}^{(1)}\right)}{\tilde{n}\left(l_{\mathrm{dsDNA}}^{(2)}, l_{\mathrm{ssDNA}}^{(2)}\right)}. \qquad [11]$$

In other words, the relative potency of both diFabs is determined solely by the separation distances between the two Fabs in the diFabs, so that the entropy, rather than the energy, determines which diFab will be more effective.

When the linker in a diFab becomes too small ($l_{\mathrm{dsDNA}} \lesssim l_{\mathrm{linker}} - l_{\mathrm{flex}}$) or too large ($l_{\mathrm{dsDNA}} \gtrsim l_{\mathrm{linker}} + l_{\mathrm{flex}}$), the diFab loses the ability to bind bivalently ($n(l_{\mathrm{dsDNA}}) \approx 0$) and the $\mathrm{IC}_{50}$ attains a constant value

$$\mathrm{IC}_{50} \approx K_{\mathrm{D}}^{(1)} \quad (\text{far from optimal geometry}) \qquad [12]$$

shown as a pink dashed line in Fig. 2D, which is roughly consistent with neutralization data for long and short diFabs.

**Altering the Fraction of ssDNA and dsDNA in the Linker**

We next investigated how well the probability of diFab binding (Eq. 9) quantitatively characterized the neutralization of new diFab constructs. We first tuned the rigidity of the linker while keeping the length of the DNA segment fixed. Starting with the optimal construct (*d*=62, *s*=12), five new diFabs were created with different amounts of dsDNA *d* flanked by two ssDNA segments *s* maintaining *d*+2*s*=86 bases (Fig. 3A), and their neutralization of HIV-1 strain 6535.3 was assessed using an in vitro neutralization assay (Fig. 3B; Table 2). We found that increasing the fraction of ssDNA from the optimal (*d*=62, *s*=12) diFab decreased potency; e.g., changing *d*=62 bp to *d*=58 bp decreased the potency by 4-fold ($\mathrm{IC}_{50}$ = 2.0 nM for (*d*=58, *s*=14) compared with 0.5 nM for (*d*=62, *s*=12)), while constructs with $d \leq 50$ exhibited uniformly poor neutralization ($\mathrm{IC}_{50}$ values >30 nM), suggesting that each of the latter constructs could only bind monovalently. Similar trends were observed for the potencies of the new diFabs against a different HIV-1 strain, THRO4156 (Appendix E Fig. S7), suggesting that ssDNA bases cannot compensate for the optimal 62 bp length of dsDNA in the linker of a 3BNC60 diFab.

The drop in diFab efficacy when ssDNA is traded for dsDNA is surprising considering that free ssDNA has a persistence length of 2-6 bases (43, 44), so that constructs such as (*d*=62, *s*=12) and (*d*=58, *s*=14) might be predicted to behave nearly identically, with the extra flanking ssDNA compensating for the shorter dsDNA. Indeed, when the flanking ssDNA is modeled with a

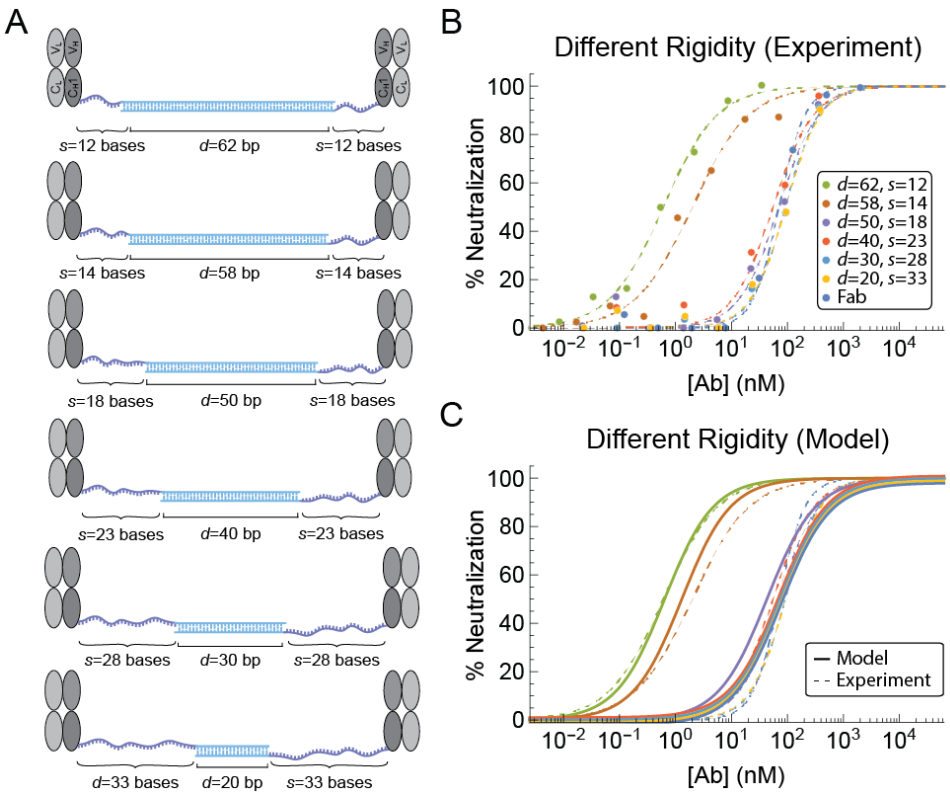


**Fig. 3. Effects of linker rigidity on diFab potency.** (A) Schematics of 3BNC60 diFabs with different proportions of dsDNA and ssDNA in their linkers. The linkers were constructed to span 86 bases of DNA, of which *d* = 62, 58, 50, 40, 30, or 20 bases were dsDNA. (B) Experimental results from in vitro neutralization assays comparing potencies of diFabs shown in panel A against HIV-1 strain 6535.3 (data points represent the average of duplicate measurements). (C) For clarity, we compare the model results (solid lines) to the experimental best-fit curves (dashed lines). See Table 2 for $IC_{50}$ values derived from the theoretical and experimental curves.

persistence length of 2 bases, the *d*=62 bp, *d*=58 bp, and *d*=50 bp constructs exhibit similar potencies (Appendix D Figure S5B) in contrast to the experimental results in which the *d*=58 bp and *d*=50 bp diFabs were less potent. Taken together with the DLS measurements (Fig. 1D), these results provide further justification for the idea that the ssDNA diFabs exhibit a shorter persistence length than free ssDNA. Indeed, the $IC_{50}$ values for the rigidity diFabs (Fig. 3A; Table 2) were nearly identical to the corresponding constructs with the same number of dsDNA bps but different lengths of ssDNA (Fig. 1B and Table 1), demonstrating that the amount of ssDNA negligibly influenced the neutralization potency of the diFab. Using the same parameters as in Fig. 2D, we found the best agreement between the experimental neutralization curves (dashed) and the model (solid lines) using a persistence length of 0.1 nm (Fig. 3C). Using the model to extrapolate to other diFabs in this family with *d* bp dsDNA and *s*=(86-*d*)/2 bases ssDNA led to nearly identical results to those shown in Fig. 2D (black line) for constructs with the same *d* but *s*=12; the $IC_{50}$ quickly increased as dsDNA was traded for ssDNA and saturated at *d*≈50 to the value $K_D^{(1)} = 74$ nM.

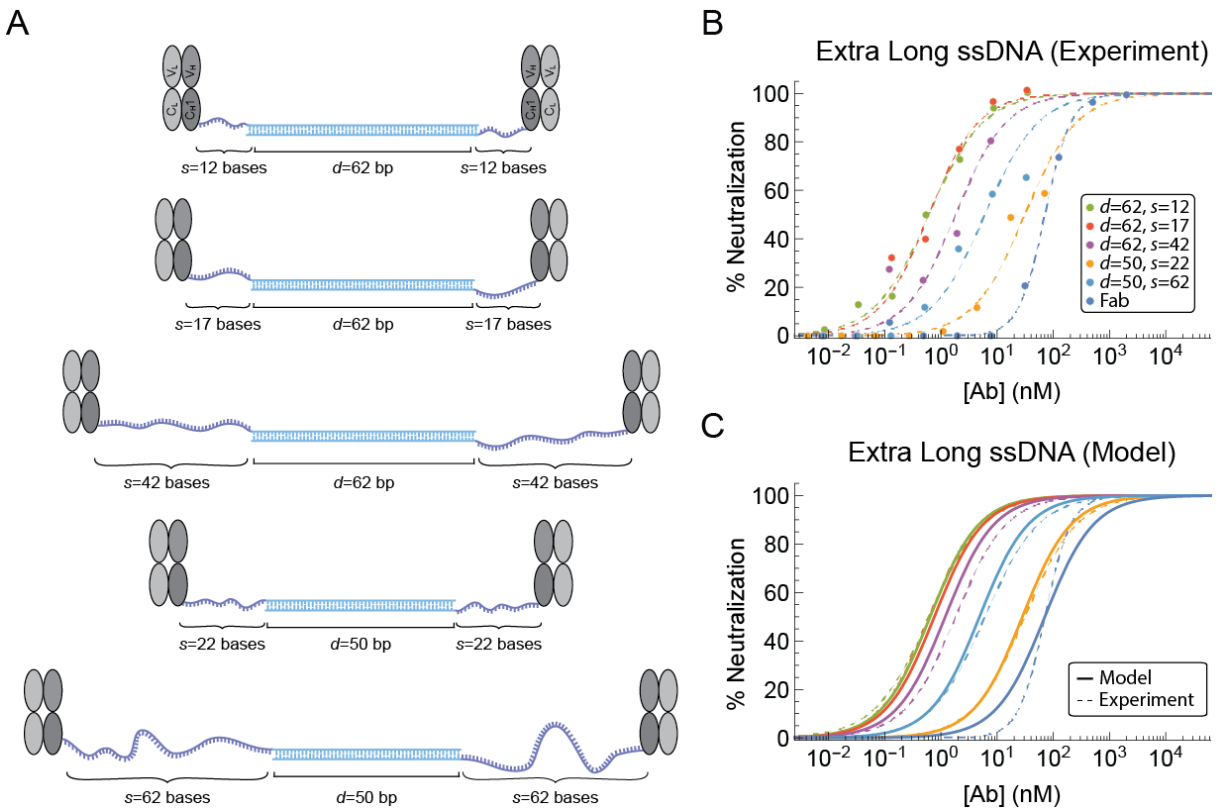


**Fig. 4. Effects of extra long ssDNA in linkers on diFab potency.** (A) Schematics of 3BNC60 diFabs. (B) Experimental in vitro neutralization assays against HIV-1 strain 6535.3 (data points represent the mean of duplicate measurements). (C) Comparison of experimental results (dashed lines) with the model (solid lines). See Table 2 for $IC_{50}$ values derived from the theoretical and experimental curves.

### Extra Long ssDNA Segments are Characterized by a Short Persistence Length

Because the length of ssDNA in the previous constructs minimally affected diFab potency, we constructed diFabs with extra long ssDNA regions to test whether the ssDNA in this limit has an appreciable effect (Fig. 4A; Table 2). If the size of the ssDNA grows slowly with its length, we would expect that constructs with increased ssDNA, such as (*d*=62, *s*=17) and (*d*=62, *s*=42), would neutralize less potently than their counterpart (*d*=62, *s*=12) with the same length of dsDNA. We found linkers with a relatively short ssDNA flanking region had similar potencies, $IC_{50}$ = 0.5 nM (*d*=62, *s*=12) and $IC_{50}$ = 0.6 nM (*d*=62, *s*=17), which slightly decreased when a larger amount of ssDNA was added to the optimal *d*=62 bp linker, $IC_{50}$ = 1.8 nM (*d*=62, *s*=42) (Table 2).

On the other hand, since the size of ssDNA grows slowly with the number of bases, we would expect that the efficacy of a sub-optimal diFab such as (*d*=50, *s*=12) (Fig. 1C) would improve with longer flanking ssDNA that might be better able to compensate for the short dsDNA. Although variability in the data made it difficult to see such trends – the neutralization $IC_{50}$ counterintuitively increased from 8.5 nM (*d*=50, *s*=12) to 31 nM (*d*=50, *s*=22) before decreasing as expected to 6.1 nM (*d*=50, *s*=62) – the model predicts that the $IC_{50}$ values should continually decrease as ssDNA is added, although this effect is minimal. More precisely, the predicted $IC_{50}$ = 69 nM for (*d*=50, *s*=12) should monotonically decrease until it hits the minimum value $IC_{50}$ = 3 nM for (*d*=50, *s*=200), past which point the $IC_{50}$ will slowly increase as the ssDNA makes the diFab too long to optimally bind bivalently. Taken together, these results emphasize that while

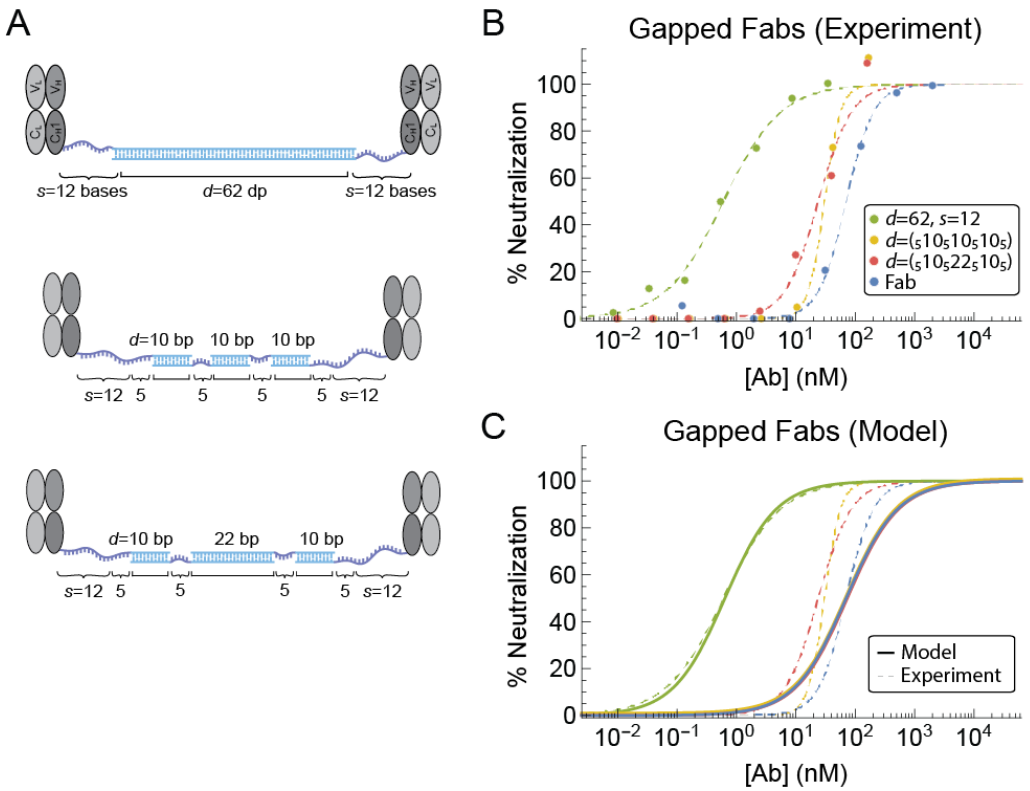


**Fig. 5. Effects of gaps in dsDNA portions of diFab linkers on potency.** (A) Schematics of 3BNC60 diFabs with ssDNA gaps interspersed within the dsDNA portion of the linker. (B) Experimental in vitro neutralization assays against HIV-1 strain 6535.3 show that these diFabs neutralize weakly (data points represent the average of duplicate measurements). (C) Comparison of experimental results (dashed lines) with the model presented in Appendix F (solid lines). See Table 2 for $IC_{50}$ values derived from the theoretical and experimental curves.

the ssDNA may play a minor role in determining a diFab's efficacy, the length of the rigid dsDNA is the single most important factor that determines diFab potency.

**Adding ssDNA Gaps makes dsDNA Flexible and Decreases diFab Efficacy**

As a final probe of the effects of linker flexibility, we investigated the potency of two diFabs in which the dsDNA linker was interspersed with short ssDNA segments (Fig. 5A; Table 2). These constructs, denoted by ($_5$10$_5$10$_5$10$_5$) and ($_5$10$_5$22$_5$10$_5$), contained the same lengths of DNA as (*d*=50, *s*=12) and (*d*=62, *s*=12) in Table 1. However, the dsDNA in ($_5$10$_5$10$_5$10$_5$) and ($_5$10$_5$22$_5$10$_5$) was flanked by an extra 5 bases of ssDNA on both sides and interrupted in two places by 5 bases of ssDNA. Both new constructs neutralized HIV-1 strain 6535.3 only weakly with $IC_{50}$ values >30 nM, by contrast to their counterparts, which had $IC_{50}$ values of 8.5 nM for (*d*=50, *s*=12) and <1 nM for the optimal (*d*=62, *s*=12) construct (Tables 1 and 2). These results again emphasize that optimal neutralization potency for a 3BNC60 diFab requires a rigid linker that spans a distance dictated by 62 bp and show that interrupting a diFab with a sub-optimal 50 bp dsDNA linker with flexible ssDNA further decreases its potency.

Our model can be generalized to analyze these constructs by considering the inner ssDNA segments as simple hinges with no length so that the dsDNA can now be characterized as a random walk composed of three steps (Appendix F). The two outer ssDNA segments can be modeled as a random walk with a persistence length of 0.1 nm. For the larger of the two

constructs, ($_5$10$_5$22$_5$10$_5$), the 42 bp of dsDNA would account for a maximum of only 14 nm when arranged linearly, thus the two outer ssDNA segments would have to stretch outwards by at least 7 nm (11 bases) to achieve the optimal separation distance of 21 nm in the unlikely event that all of the DNA segments were colinear. The shorter construct in Fig. 5A ($_5$10$_5$10$_5$10$_5$) would require the ssDNA to stretch even further to achieve maximal potency. Hence, the two gapped diFabs should only bind monovalently with an $IC_{50}$ given by Eq. 12, as confirmed by the data and model in Fig. 5B,C and Table 2. Note that even if the dsDNA region of the linker were made longer, increasing the dsDNA flexibility in this manner increases the entropy lost when going from the monovalently- to bivalently-bound states and hence decreases the neutralization potency of the diFab. In Appendix F, we use the model to quantify the decrease in potency as the dsDNA in the optimal ($d$=62, $s$=12) construct is broken into multiple segments.

## Discussion

The low density of Env spikes on HIV-1 potentially enables the virus to mitigate the host antibody response by hindering host IgGs from using both antigen-binding Fabs to bind bivalently, thereby expanding the range of HIV-1 mutations permitting antibody evasion (21, 22). The observation that a mutant simian immunodeficiency virus (SIV) with a higher number of Env spikes reverted to its normal spike number of ≈14 when propagated in non-human primate hosts is consistent with selection against those viruses that facilitate the ability of host IgGs to bind bivalently through inter-spike crosslinking (55). Although HIV-1 may be more infectious and hence spread more rapidly with more Env trimers (56), the immune system apparently applies selective pressure that keeps the Env spike count per virion low, presumably to prevent anti-HIV-1 IgGs from utilizing avidity effects to counter the lower intrinsic Fab-Env affinities that result from rapid mutation of Env. Antibody isotypes such as dimeric IgA or pentameric IgM have increased valencies (four and ten Fabs, respectively) compared to the two Fabs of an IgG, thus allowing for increased avidity effects during antibody binding to a pathogen. However, most of the neutralizing activity in the sera of HIV-1–positive individuals is attributed to IgGs (57, 58), and converting an anti-HIV-1 IgG broadly neutralizing antibody to an IgA or IgM has minimal effects on potency in standard neutralization assays (59, 60). Thus, most antibodies against HIV-1 Env must resort to monovalent binding by IgGs in the absence of avidity effects that would strengthen their interactions with other pathogens.

Bivalent binding to single Env trimers is another way to utilize avidity effects to counteract the low spike density of HIV-1. Although the architecture of HIV-1 Env trimers prohibits simultaneous binding of both Fabs of conventional, host-derived IgGs (29, 30), we constructed synthetic antibodies (Fig. 1B) (diFabs constructed from Fabs from a neutralizing anti-HIV-1 IgG joined by a linker containing rigid dsDNA flanked by flexible ssDNA) designed to achieve intra-spike crosslinking; i.e., bivalent binding to adjacent Fab binding sites on a single Env trimer. In previous work, we measured the neutralization potencies of an array of diFabs with different dsDNA lengths and found that the linker in the optimal 3BNC60 diFab had 62 bp (21 nm) dsDNA.

The optimal 21 nm length of the dsDNA portion of the linker can be compared to the distance between adjacent 3BNC60 Fabs in various conformations of HIV-1 Envs. It has been shown that HIV-1 Env trimers adopt multiple conformations on virions (24, 61) and in the soluble native-like forms used for structural studies (48). For example, binding of the host CD4 receptor induces outward displacements of the three Env gp120 subunits, resulting in an open conformation in which the coreceptor binding sites on the trimer apex V3 loops are exposed (62-65) and which rearranges further upon coreceptor binding and subsequent membrane fusion.

We measured the distances between adjacent 3BNC60 epitopes on Env trimers in different conformations using a new cryo-EM structure of 3BNC117 Fab (a close relative of 3BNC60 (37)) bound to a closed Env trimer (66). Measurements from this single-particle cryo-EM structure allows estimation of the average position of the C-terminal $C_H1$ domain residue to which the DNA in our diFabs was covalently attached, since Fabs in cryo-EM structures are not influenced by crystal packing forces that can alter the $C_H1$-$C_L$ domain position relative to the $V_H$-$V_L$ domains in X-ray structures (47). We used the 3BNC117 Fab-gp120 portion of the cryo-EM structure to measure the distance between adjacent Fab $C_H1$ C-termini in the closed conformation of Env and then modeled a 3BNC60-gp120 protomer into three recent cryo-EM structures of Env trimers in different conformations: an open Env bound by the b12 bNAb in which the coreceptor binding sites on the V3 loops are not exposed (63), an open CD4-bound Env structure with exposed V3 loops (63), and a partially-open CD4-bound Env in which the gp120 subunits adopted positions mid-way between closed and fully open (64). From these structures, we measured distances of 15.8, 20.3, 20.4, and 20.1 nm between C-termini of 3BNC60 Fab $C_H1$ domains modeled onto the closed, b12-bound open, CD4-bound open, and CD4-bound partially-open Env conformations, respectively (see Methods). Although monovalent CD4-binding site bNAb Fabs bind the closed Env trimer conformation (48), the 21 nm length of the dsDNA in the optimal ($d$=62, $s$=12) diFab more closely matched measured distances for the open Env trimer structures, perhaps indicating that the diFab captured an open Env conformation that could be neutralized potently by a reagent binding through intra-spike crosslinking.

To further probe the result that an optimal linker has 62 bp dsDNA, we created an array of diFabs with variable amounts of rigid dsDNA and flexible ssDNA (Tables 1 and 2), enabling us to tune both the length and rigidity of the DNA linker. In order to provide a conceptual framework to understand how these synthetic antibodies function, we developed a statistical mechanics-based model to predict diFab potencies for inhibiting infection of the 6535.3 strain of HIV-1. By assuming that (*i*) each homotrimeric spike is unable to help infect a host cell when any one of its three epitopes are bound by Fab, and (*ii*) that the infectivity of a virion varies linearly with the number of unbound Env, we showed that the neutralization of a virion is proportional to the probability that any single Env protein is bound by a Fab (Appendix A). DLS measurements confirmed that the hydrodynamic radii of the diFabs was determined by the length of their rigid dsDNA and essentially independent of the length of ssDNA (Fig. 1D). Consequently, these constructs were best characterized by modeling the ssDNA with a smaller persistence length to account for the DLS data (Fig. 2D). This framework enabled us to translate the linker-dependent entropy and energy of binding to an HIV-1 Env trimer into a predicted neutralization potency for each diFab.

The first set of diFabs we created explored the effects of linker rigidity. These constructs had the same total length of DNA (86 bases) but differed in their fractions of dsDNA and ssDNA (Fig. 3). We found that as the dsDNA decreased from the optimal $d$=62 to $d$=58, 50, 40, 30, and 20 bp, the potency of the antibodies rapidly decreased so that the four constructs with $d \leq 50$ neutralized only as effectively as the monovalent Fab. From a modeling perspective, the short ssDNA persistence length implies that the ssDNA plays a minor role in determining diFab potency. Hence, the constructs composed of $d$ bp dsDNA and $s$=(86-$d$)/2 bases ssDNA should behave similarly to the constructs with $d$ bp dsDNA and $s$=12 bases ssDNA in Fig. 1C and Table 1, as verified experimentally by comparing $IC_{50}$s of constructs with the same dsDNA lengths (Tables 1 and 2). In other words, decreasing the dsDNA length shortened the length of the diFabs to the point where only monovalent binding was possible when $d \leq 50$.

A second set of diFabs explored whether extra long ssDNA segments can alter diFab potency (Fig. 4). The observed effects were minor; for example, the observed $IC_{50}$ = 0.5 nM of the optimal construct (*d*=62, *s*=12) slightly decreased when 30 bases of ssDNA were added to both flanking ssDNA segments, resulting in an $IC_{50}$ = 1.8 nM for (*d*=62, *s*=42) (Table 2). These results reaffirm that the length of dsDNA in the linker has greater impact on diFab potency than the length of ssDNA.

Finally, we considered two additional diFabs that introduced ssDNA gaps within the dsDNA portion of the linker (Fig. 5). Both constructs exhibited poor neutralization potencies comparable to that of a monovalent Fab. Our model affirmed that introducing flexibility into the dsDNA in this manner increases the entropic cost of bivalently binding (see Appendix F).

Although our model successfully reproduced the neutralization curves of the new synthetic diFabs evaluated here, we point out several factors of the HIV-1 system that the model neglects. First, the model does not consider potential diFab binding between adjacent Env trimers, although this binding should be minimal given the low density of Env on the virion's surface. Second, our model assumed that the % neutralization of HIV-1 decreases linearly with the number of unbound Env trimers (Appendix A); such a linear relationship has been observed when less than half the HIV-1 spikes are bound (56), although it may not hold when more than half of the spikes are bound (possibly because some minimum number of unbound Env trimers are needed to successfully infect a cell). In a similar vein, we neglected the variability in the numbers of spikes per virion (23-26), instead assuming that all virions had exactly 14 spikes. However, relaxing these assumptions yielded nearly identical results (Appendix A), suggesting that the model is robust to these assumptions.

A compelling extension of this work that would deepen our understanding of the antibody response against HIV-1 would be to consider reagents with more than two Fabs. As has been seen in other biological systems (67-69), synthetic antibodies with greater valency can elicit tighter binding. Hence, a triFab that allows three Fabs to simultaneously bind to an HIV-1 Env trimer is predicted to have a lower $IC_{50}$ than an optimal diFab; indeed, our model predicts that an optimal triFab would have an $IC_{50}$ that is 100x more potent than the optimal (*d*=62, *s*=12) diFab (see Appendix F). Modeling verifies that a rigid linker is required for a bivalent or trivalent reagent to achieve avidity effects by intra-spike crosslinking, thus providing guidance for constructing optimal anti-HIV-1 therapeutics that remain potent against HIV-1 in the face of the Env mutations arising during HIV-1 replication.

Multivalency has been harnessed in an array of fields that extend beyond immunology; e.g., novel materials and scaffolds have been designed at the super-cellular scale using multivalency (70), and molecular targeting and molecular machines employ multivalency at the molecular scale (69, 71, 72). We hope that our work presents a step towards precise, quantitative models that encompasses multivalent binding in each of these contexts.

## Methods

### Expression and Purification of Fabs

The gene encoding the 3BNC60 light chain was modified using site-directed mutagenesis to remove the C-terminal cysteine that forms a disulfide bond with the Fab heavy chain, leaving a single free cysteine at the C-terminus of the Fab heavy chain as described (21). Modified light chain genes and genes encoding 6xHis-tagged 3BNC60 Fab heavy chains ($V_H$–$C_H$1–tag) were subcloned separately into the pTT5 mammalian expression vector (NRC Biotechnology Research Institute). 3BNC60 Fabs and IgG were expressed by transient transfection in HEK 293-6E (NRC Biotechnology Research Institute) cells as described (73) and purified from supernatants by Ni-NTA affinity chromatography followed by size exclusion chromatography in PBS pH 7.4 using a Superdex 200 10/300 or Superdex 200 16/600 column (Amersham Biosciences).

### DNA Conjugation to Fabs

ssDNA was synthesized, phosphorylated, and PAGE purified by Integrated DNA Technologies and conjugated to modified 3BNC60 Fab using a previously-described protocol (21). Briefly, 3BNC60 Fab was reduced in buffer containing 10mM TCEP-HCl pH 7-8 for two hours, and then buffer exchanged three times over Zeba desalting columns (Thermo Scientific). The percentage of reduced Fab was determined using Measure-IT Thiol Assay (Invitrogen). Concurrently, ssDNA containing a 5' amino group (Integrated DNA Technologies, IDT-DNA) was incubated with a 100-200–fold molar excess of Sulfo-SMCC, an amine-to-sulfhydryl crosslinker (Thermo Scientific) for 30 minutes to form a maleimide-activated DNA strand, which was buffer exchanged as described above and incubated overnight. The Fab-ssDNA conjugate was purified by anion exchange chromatography using MonoQ resin (GE Biosciences) to separate unreacted Fab and ssDNA from the conjugate.

The NUPACK server (74) was used to predict thermally-stable DNA sequences lacking secondary structures to make dsDNA bridges. Bridge and linker sequences are listed in Table S4 (Appendix G). For di-Fabs containing dsDNA bridges longer than 40bp, complementary ssDNAs were annealed by heating (95°C) and cooling (room temperature) to create dsDNA containing overhangs complementary to the Fab-ssDNA conjugates. dsDNA was purified by size exclusion chromatography (Superdex 200 10/300) and incubated overnight with the corresponding tagged Fab-ssDNA conjugates. DiFab reagents were purified by Ni-NTA affinity chromatography to remove free DNA and excess Fab-ssDNA conjugates, treated with T4 DNA ligase (New England Biolabs), and purified again by size exclusion chromatography. To make di-Fabs containing dsDNA bridge lengths less than 40bp or containing gapped sequences, two complementary ssDNA-conjugated Fabs were incubated at 37°C without a dsDNA bridge and then purified as described above. Protein-DNA reagents were stable at 4°C for >6 months as assessed by SDS-PAGE.

### Characterization of DNA-Fab Reagents

Fractions from the center of an SEC elution peak were concentrated using Amicon Ultra-15 Centrifugal Filter Units (Millipore) (MW cutoff = 10 kDa) to a volume of 500 µL. DLS measurements were performed on a DynaPro NanoStar DLS instrument (Wyatt Technology) using the manufacturer's suggested settings (10 acquisitions/measurement). Autocorrelation data were fit using the Dynamics software package with the globular protein MW-R model and compared using both cumulant and regularization fits to give a hydrodynamic radius for each diFab. Three independent DLS measurements were performed for each sample and the results were averaged.

**In Vitro Neutralization Assays**

The 6535.3 pseudovirus for in vitro neutralization assays was generated by co-transfecting HEK293T cells with vectors encoding Env and a replication-deficient HIV-1 backbone (obtained from the Fraunhofer Institute IBMT) as described (40). Neutralization was monitored by the reduction of HIV-1 Tat-induced luciferase reporter gene expression in the presence of a single round of pseudovirus infection in TZM-bl cells using a protocol modified from (40). To avoid false positive neutralization signals from dsDNA-containing reagents potentially due to the inclusion of DEAE-dextran, which can interact with DNA (75), we eliminated DEAE-dextran from the assays in which the dsDNA linker alone reduced infectivity and increased the pseudovirus concentration by 2.5–40-fold as described (21). Comparisons of $IC_{50}$ values for 3BNC60 IgG and Fab derived from neutralization assays conducted in the presence and absence of DEAE-dextran showed no systematic differences (unpublished results).

Some of the neutralization data were derived from neutralization assays prepared by a Freedom EVO® (Tecan) liquid handler ($IC_{50}$ values derived from manual and robotic assays agreed to within 2-4 fold; unpublished results). Reagents (3-, 4-, or 5-fold dilution series; each concentration in duplicate) were incubated with 250 (when DEAE dextran was added) or >1000 (when DEAE dextran was not added) viral infectious units at 37°C for one hour prior to incubation with reporter cells (10,000/well) for 48 hours. Luciferase levels were measured from a cell lysate using an Infinite 200 Pro microplate reader (Tecan) after addition of BrightGlo (Promega). For constructs where multiple replicates of the neutralization curves were measured, a representative curve whose $IC_{50}$ was closest to the mean value is shown in Figs. 3-5.

**Fitting Neutralization Assays**

Data were first analyzed using HIV Antibody Database (76) and then fit using nonlinear regression to the 2-parameter Hill function

$$\frac{\left(\frac{[\mathrm{Ab}]}{\mathrm{IC}_{50}}\right)^{n}}{1+\left(\frac{[\mathrm{Ab}]}{\mathrm{IC}_{50}}\right)^{n}} \qquad [13]$$

to derive experimental $IC_{50}$ values (Table 2). The $IC_{50}$ values in Table 1 were previously reported and determined in as described (21).

The equilibrium dissociation constant $K_D^{(1)}$ characterizing the binding of the first diFab arm to HIV-1 Env (which is equivalent to the dissociation constant between a diFab with only one functional arm) is equal to the dissociation constant between a Fab and HIV-1 Env. We assumed that the Fab's neutralization potency was proportional to its ability to bind Env. Therefore, rather than fitting $K_D^{(1)}$, we set it to equal the $IC_{50}$ value for the in vitro neutralization assay of the monovalent Fab, namely, $K_D^{(1)} = 74 \pm 31$ nM (*n*=13 replicates). The remaining parameters (e.g., $l_{\mathrm{linker}}$, $l_{\mathrm{flex}}$, $\xi_{\mathrm{ssDNA}}$, $\alpha$, $\tilde{\alpha}$) were determined using nonlinear regression using the neutralization curves for all constructs (see Appendix D and the Supporting Information Mathematica notebook where the raw data, the fitting, and the figures are reproduced).

**Measurements of Separation Distances on Env Trimer Structures**

We used a single-particle cryo-EM structure (66) of a closed Env trimer bound to 3BNC117, a 3BNC60-related bNAb (37) for estimating the position of position of $C_H1$ residue 233 (to which the DNA linker in the 3BNC60 diFabs was attached) when a 3BNC60 diFab is bound to an Env trimer. The coordinates for the $V_H$-$V_L$ domains of the 3BNC60 Fab (37) were superimposed on

the 3BNC117 $V_H$-$V_L$ domains, and the coordinates for the $C_H1$-$C_L$ domains from the structure of b12 IgG (28) were superimposed on the 3BNC117 $C_H1$-$C_L$ domains because $C_H1$ residues 217 – 233 are disordered in the 3BNC60 Fab structure (37). The model for the 3BNC60 Fab-gp120 portion of the trimeric cryo-EM complex structure was used to measure the distance between adjacent Fab $C_H1$ C-termini in the closed conformation of Env and then modeled into three cryo-EM structures of Envs in different conformations: an open Env bound by the b12 bNAb in which the coreceptor binding sites on the V3 loops are not exposed (63), an open CD4-bound Env structure with exposed V3 loops (63), and a partially-open CD4-bound Env in which the gp120 subunits adopted positions mid-way between closed and fully open (64).

## Author Contributions

R.P.G., T.E., A.P.W., R.P. and P.J.B. conceived the project and interpreted data; R.P.G. designed, constructed, and characterized diFabs; T.E., S.Y., and R.P developed the model and performed analyses; P.N.P.G. and A.M.L. performed in vitro neutralization assays; D.S.J, and A.M.L. assisted with diFab construction; T.E., R.P., and P.J.B. wrote the paper with input from other authors.

## Acknowledgements

We thank Anthony Bartolotta, Justin Bois, Jim Eisenstein, Vahe Galstyan, Peng He, Willem Hegel, David Hsieh, Giacomo Koszegi, Pankaj Mehta, Jiseon Min, Olexei Motrunich, Noah Olsman, Vahe Singh, and Richard Zhu for useful discussions, Christopher Barnes for measuring modeled 3BNC60-Env complexes, Aaron Coey for discussions about triFabs $IC_{50}$s, and affinities, and Marta Murphy for help with preparing figures. This research was supported by National Institute of Allergy and Infectious Diseases of the National Institutes of Health grants 1R01AI129784 and HIVRAD P01 AI100148 (P.J.B.), the Bill and Melinda Gates Foundation Collaboration for AIDS Vaccine Discovery Grant 1040753 (P.J.B.), La Fondation Pierre-Gilles de Gennes (R.P.), the Rosen Center at Caltech (R.P.), the National Institutes of Health DP1 OD000217 (Director's Pioneer Award), R01 GM085286, and 1R35 GM118043-01 (MIRA) (R.P.), and a Caltech-COH Biomedical Research Initiative (to P.J.B.). We are grateful to the Burroughs-Wellcome Fund for its support of the Physiology Course at the Marine Biological Laboratory, where part of the work on this work was done, and for a post-course research grant (S.Y.).

| Construct | Schematic | dsDNA (*d*) | ssDNA (*s*) | Experimentally Measured $IC_{50}$ (nM) | Theoretically Predicted $IC_{50}$ (nM) |
|---|---|---|---|---|---|
| Fab |  | --- | --- | 27 | |
| IgG | 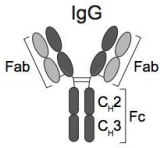 | --- | --- | 4.0 | |
| *Rigidity Constructs (Fig. 1C, Fig. 3)* | 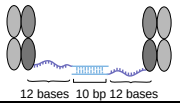 | 10 | 12 | 35 | 74 |
| | 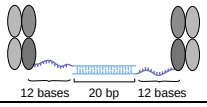 | 20 | 12 | 22 | 74 |
| | 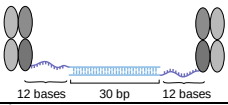 | 30 | 12 | 24 | 74 |
| | 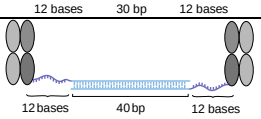 | 40 | 12 | 13 | 74 |
| | 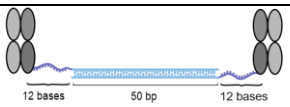 | 50 | 12 | 8.5 | 69 |
| | 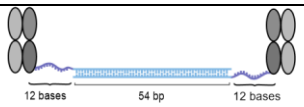 | 54 | 12 | 2.4 | 13 |
| | 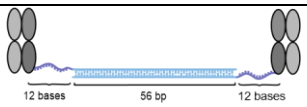 | 56 | 12 | 2.0 | 3.6 |
| | 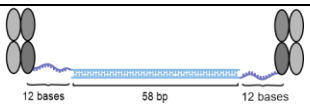 | 58 | 12 | 1.2 | 1.4 |
| | 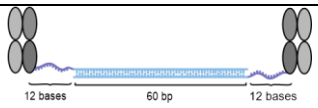 | 60 | 12 | 0.82 | 0.8 |
| | 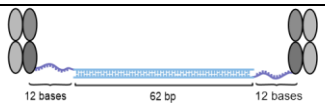 | 62 | 12 | 0.24 | 0.6 |
| | 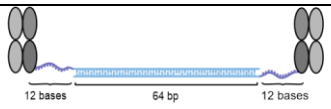 | 64 | 12 | 0.5 | 0.8 |

| | | | | | |
|---|---|---|---|---|---|
| | 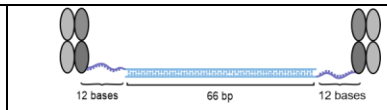 | 66 | 12 | 1.3 | 1.7 |
| | 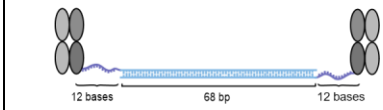 | 68 | 12 | 5.2 | 4.9 |
| | 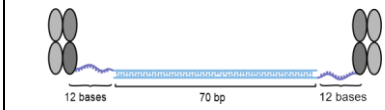 | 70 | 12 | 8.5 | 18 |
| | 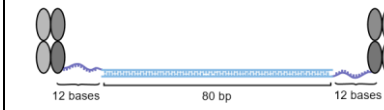 | 80 | 12 | 15 | 74 |
| | 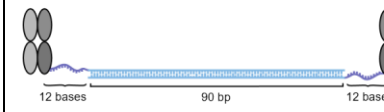 | 90 | 12 | 37 | 74 |
| | 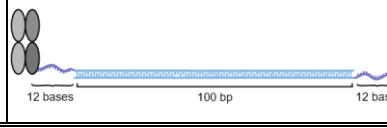 | 100 | 12 | 82 | 74 |

**Table 1: Experimental and theoretically-determined $IC_{50}$s for diFabs with linkers containing *s* = 12 bases of flanking ssDNA and different lengths of dsDNA.**
Experimentally-determined $IC_{50}$ values for 3BNC60 Fab, 3BNC60 IgG, and 3BNC60 diFabs as reported in (21). diFabs were composed of *d* bp dsDNA flanked on both sides by *s* = 12 ssDNA bases.

| Construct | Schematic | dsDNA (*d*) | ssDNA (*s*) | Experimentally Measured $IC_{50}$ (nM) | Theoretically Predicted $IC_{50}$ (nM) |
|---|---|---|---|---|---|
| Fab |  | --- | --- | 74 ± 31 (*n*=13) | |
| IgG | 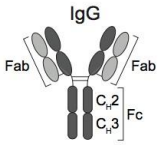 | --- | --- | 4.3 ± 0.8 (*n*=14) | |
| 3BNC60-62bp-3BNC60 | 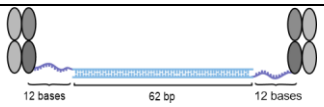 | 62 | 12 | 0.5 ± 0.15 (*n*=5) | 0.6 |
| *Rigidity Constructs (Fig. 3)* | 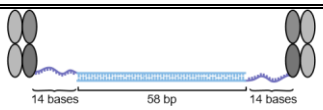 | 58 | 14 | 2.0 | 1.3 |
| | 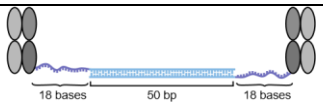 | 50 | 18 | 48 ± 32 (*n*=2) | 43 |
| | 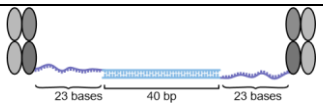 | 40 | 23 | 45 ± 15 (*n*=2) | 74 |
| | 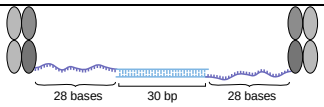 | 30 | 28 | 67 ± 36 (*n*=2) | 74 |
| | 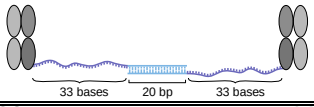 | 20 | 33 | 70 ± 33 (*n*=2) | 74 |
| *Extra Long Constructs (Fig. 4)* | 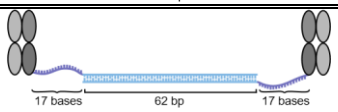 | 62 | 17 | 0.6 | 0.8 |
| | 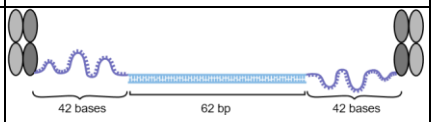 | 62 | 42 | 1.8 | 1.2 |
| | 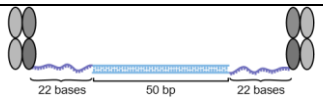 | 50 | 22 | 31 | 28 |
| | 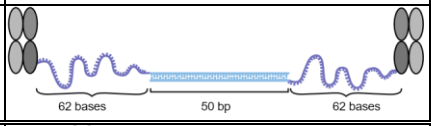 | 50 | 62 | 6.1 | 4.9 |
| *Gapped Constructs (Fig. 5)* | 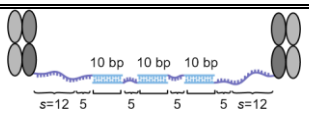 | $_5 10_5 10_5 10_5$* | 12 | 30 | 74 |

| | | | | | |
|---|---|---|---|---|---|
| | 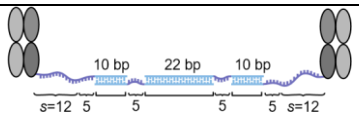 | $_{5}10_{5}22_{5}10_{5}$* | 12 | 24 | 74 |

* subscript denotes flanking ssDNA length

**Table 2: Experimental and theoretically-determined $IC_{50}$s for new diFabs.** 3BNC60 diFabs were composed of *d* bp dsDNA flanked on both sides by *s* bases of ssDNA. Gapped diFabs (Fig. 5) are denoted by the lengths of their dsDNA segments with subscripts representing inserted ssDNA bases. Experimentally-determined $IC_{50}$ values for 3BNC60 Fab, 3BNC60 IgG, and (*d*=62, *s*=12) diFab are reported as the mean and standard deviation for 3BNC60 Fab (n = 13 independent experiments), 3BNC60 IgG (14 independent experiments), the optimal (*d*=62, *s*=12) diFab (5 independent experiments), and four of the new diFabs (2 independent experiments), and as one value when a single neutralization experiment was conducted.

## References

1. UNAIDS (2017) UNAIDS Data 2017.
2. Fauci AS (2008) 25 years of HIV. Nature 453(7193):289-90.
3. Escolano A, Dosenovic P, Nussenzweig MC (2017) Progress toward active or passive HIV-1 vaccination. J Exp Med 214(1):3-16.
4. McCoy LE, Burton DR (2017) Identification and specificity of broadly neutralizing antibodies against HIV. Immunol Rev 275(1):11-20.
5. Klasse PJ (2012) The molecular basis of HIV entry. Cell Microbiol 14(8):1183-92.
6. Baba TW, Liska V, Hofmann-Lehmann R, Vlasak J, Xu W, Ayehunie S, et al. (2000) Human neutralizing monoclonal antibodies of the IgG1 subtype protect against mucosal simian-human immunodeficiency virus infection. Nat Med 6(2):200-6.
7. Mascola JR, Stiegler G, VanCott TC, Katinger H, Carpenter CB, Hanson CE, et al. (2000) Protection of macaques against vaginal transmission of a pathogenic HIV-1/SIV chimeric virus by passive infusion of neutralizing antibodies. Nat Med 6(2):207-10.
8. Hessell AJ, Rakasz EG, Poignard P, Hangartner L, Landucci G, Forthal DN, et al. (2009) Broadly neutralizing human anti-HIV antibody 2G12 is effective in protection against mucosal SHIV challenge even at low serum neutralizing titers. PLoS Pathog 5(5):e1000433.
9. Hessell AJ, Hangartner L, Hunter M, Havenith CE, Beurskens FJ, Bakker JM, et al. (2007) Fc receptor but not complement binding is important in antibody protection against HIV. Nature 449(7158):101-4.
10. Klein F, Halper-Stromberg A, Horwitz JA, Gruell H, Scheid JF, Bournazos S, et al. (2012) HIV therapy by a combination of broadly neutralizing antibodies in humanized mice. Nature 492(7427):118-22.
11. Klein F, Mouquet H, Dosenovic P, Scheid JF, Scharf L, Nussenzweig MC (2013) Antibodies in HIV-1 vaccine development and therapy. Science 341(6151):1199-204.
12. Klein F, Nogueira L, Nishimura Y, Phad G, West AP, Jr., Halper-Stromberg A, et al. (2014) Enhanced HIV-1 immunotherapy by commonly arising antibodies that target virus escape variants. J Exp Med 211(12):2361-72.
13. Caskey M, Klein F, Lorenzi JC, Seaman MS, West AP, Jr., Buckley N, et al. (2015) Viraemia suppressed in HIV-1-infected humans by broadly neutralizing antibody 3BNC117. Nature 522(7557):487-91.
14. Caskey M, Schoofs T, Gruell H, Settler A, Karagounis T, Kreider EF, et al. (2017) Antibody 10-1074 suppresses viremia in HIV-1-infected individuals. Nat Med 23(2):185-91.
15. Lynch RM, Boritz E, Coates EE, DeZure A, Madden P, Costner P, et al. (2015) Virologic effects of broadly neutralizing antibody VRC01 administration during chronic HIV-1 infection. Science translational medicine 7(319):319ra206.
16. Schoofs T, Klein F, Braunschweig M, Kreider EF, Feldmann A, Nogueira L, et al. (2016) HIV-1 Immunotherapy with Monoclonal Antibody 3BNC117 Elicits Host Immune Responses against HIV-1. Science 352(6288):997-1001.
17. Moore PL, Gray ES, Wibmer CK, Bhiman JN, Nonyane M, Sheward DJ, et al. (2012) Evolution of an HIV glycan-dependent broadly neutralizing antibody epitope through immune escape. Nat Med 18(11):1688-92.
18. Liao HX, Lynch R, Zhou T, Gao F, Alam SM, Boyd SD, et al. (2013) Co-evolution of a broadly neutralizing HIV-1 antibody and founder virus. Nature 496(7446):469-76.
19. Wibmer CK, Bhiman JN, Gray ES, Tumba N, Abdool Karim SS, Williamson C, et al. (2013) Viral escape from HIV-1 neutralizing antibodies drives increased plasma neutralization breadth through sequential recognition of multiple epitopes and immunotypes. PLoS Pathog 9(10):e1003738.

20. Doria-Rose NA, Schramm CA, Gorman J, Moore PL, Bhiman JN, DeKosky BJ, et al. (2014) Developmental pathway for potent V1V2-directed HIV-neutralizing antibodies. Nature 509(7498):55-62.
21. Galimidi RP, Klein JS, Politzer MS, Bai S, Seaman MS, Nussenzweig MC, Bjorkman, PJ (2015) Intra-spike crosslinking overcomes antibody evasion by HIV-1. Cell 160(3):433–46.
22. Klein JS, Bjorkman PJ (2010) Few and far between: how HIV may be evading antibody avidity. PLoS Pathog 6(5):e1000908.
23. Chertova E, Bess Jr JW, Jr., Crise BJ, Sowder IR, Schaden TM, Hilburn JM, et al. (2002) Envelope glycoprotein incorporation, not shedding of surface envelope glycoprotein (gp120/SU), Is the primary determinant of SU content of purified human immunodeficiency virus type 1 and simian immunodeficiency virus. J Virol 76(11):5315-25.
24. Liu J, Bartesaghi A, Borgnia MJ, Sapiro G, Subramaniam S (2008) Molecular architecture of native HIV-1 gp120 trimers. Nature 455(7209):109-13.
25. Zhu P, Chertova E, Bess J, Jr., Lifson JD, Arthur LO, Liu J, et al. (2003) Electron tomography analysis of envelope glycoprotein trimers on HIV and simian immunodeficiency virus virions. Proc Natl Acad Sci USA 100(26):15812-7.
26. Zhu P, Liu J, Bess J, Jr., Chertova E, Lifson JD, Grise H, et al. (2006) Distribution and three-dimensional structure of AIDS virus envelope spikes. Nature 441(7095):847-52.
27. Patel P, Borkowf CB, Brooks JT, Lasry A, Lansky A, Mermin J (2014) Estimating per-act HIV transmission risk: a systematic review. AIDS (London, England) 28(10):1509-19.
28. Saphire EO, Parren PW, Pantophlet R, Zwick MB, Morris GM, Rudd PM, et al. (2001) Crystal structure of a neutralizing human IgG against HIV-1: a template for vaccine design. Science 293(5532):1155-9.
29. Klein JS (2009) Investigations in the design and characterization of HIV-1 neutralizing molecules. Pasadena: California Institute of Technology.
30. Wang H, Gristick HB, Scharf L, West AP, Galimidi RP, Seaman MS, et al. (2017) Asymmetric recognition of HIV-1 Envelope trimer by V1V2 loop-targeting antibodies. Elife 6.
31. Layne SP, Merges MJ, Dembo M, Spouge JL, Conley SR, Moore JP, et al. (1992) Factors underlying spontaneous inactivation and susceptibility to neutralization of human immunodeficiency virus. Virology 189(2):695-714.
32. Eisen HN, Siskind GW (1964) Variations in Affinities of Antibodies during the Immune Response. Biochemistry 3:996-1008.
33. Azimzadeh A, Van Regenmortel MH (1990) Antibody affinity measurements. J Mol Recognit 3(3):108-16.
34. Kiessling LL, Lamanna AC (2003) Multivalency in Biological Systems. In: Schneider MP, editor. Chemical Probes in Biology NATO Science Series (Series II: Mathematics, Physics and Chemistry). 129: Springer, Dordrect.
35. Krishnamurthy VM, Estroff LA, Whitesides GM (2006) Multivalency in Ligand Design: Wiley‐VCH Verlag GmbH & Co. KGaA.
36. Karush F (1976) Multivalent binding and functional affinity. Contemp Top Mol Immunol 5:217-28.
37. Scheid JF, Mouquet H, Ueberheide B, Diskin R, Klein F, Olivera TY, et al. (2011) Sequence and Structural Convergence of Broad and Potent HIV Antibodies That Mimic CD4 Binding. Science 333:1633-7.
38. Klein JS, Jiang S, Galimidi RP, Keeffe JR, Bjorkman PJ (2014) Design and characterization of structured protein linkers with differing flexibilities. Protein Engineering, Design, and Selection 27:325-30.
39. Bednar J, Furrer P, Katritch V, Stasiak AZ, Dubochet J, Stasiak A (1995) Determination of DNA persistence length by cryo-electron microscopy. Separation of the static and dynamic contributions to the apparent persistence length of DNA. J Mol Biol 254(4):579-94.

40. Montefiori DC (2005) Evaluating neutralizing antibodies against HIV, SIV, and SHIV in luciferase reporter gene assays. Current protocols in immunology / edited by John E Coligan [et al Chapter 12:Unit 12 1.
41. Merk A, Subramaniam S (2013) HIV-1 envelope glycoprotein structure. Curr Opin Struct Biol 23(2):268-76.
42. Brunet A, Tardin C, Salomé L, Rousseau P, Destainville N, Manghi M (2015) Dependence of DNA Persistence Length on Ionic Strength of Solutions with Monovalent and Divalent Salts: A Joint Theory–Experiment Study. Macromolecules 48(11):3641-52.
43. Ambia-Garrido J, Vainrub A, Pettitt BM (2010) A model for Structure and Thermodynamics of ssDNA and dsDNA Near a Surface: a Coarse Grained Approach. Comput Phys Commun 181(12):2001-7.
44. TInland B, Pluen A, Sturm J, Weill G (1997) Persistence Length of Single-Stranded DNA. Macromolecules 30(19):5763–5.
45. Doi M, Edwards SF (1986) Static Properties of Polymers. The Theory of Polymer Dynamics. Oxford, UK: Oxford University Press.
46. Dev S, Surolia A (2006) Dynamic light scattering study of peanut agglutinin: size, shape and urea denaturation. Journal of biosciences 31(5):551-6.
47. Stanfield RL, Zemla A, Wilson IA, Rupp B (2006) Antibody elbow angles are influenced by their light chain class. J Mol Biol 357(5):1566-74.
48. Ward AB, Wilson IA (2017) The HIV-1 envelope glycoprotein structure: nailing down a moving target. Immunol Rev 275(1):21-32.
49. Brandenberg OF, Magnus C, Rusert P, Gunthard HF, Regoes RR, Trkola A (2017) Predicting HIV-1 transmission and antibody neutralization efficacy in vivo from stoichiometric parameters. PLoS Pathog 13(5):e1006313.
50. Brandenberg OF, Magnus C, Rusert P, Regoes RR, Trkola A (2015) Different infectivity of HIV-1 strains is linked to number of envelope trimers required for entry. PLoS Pathog 11(1):e1004595.
51. Klasse PJ (2007) Modeling how many envelope glycoprotein trimers per virion participate in human immunodeficiency virus infectivity and its neutralization by antibody. Virology 369(2):245-62.
52. Yang X, Kurteva S, Ren X, Lee S, Sodroski J (2005) Stoichiometry of envelope glycoprotein trimers in the entry of human immunodeficiency virus type 1. J Virol 79(19):12132-47.
53. Phillips R, Kondev J, Theriot J, Garcia HG (2013) Physical Biology of the Cell. Second ed. London and New York: Garland Science (Taylor & Francis Group).
54. Lyumkis D, Julien JP, de Val N, Cupo A, Potter CS, Klasse PJ, et al. (2013) Cryo-EM structure of a fully glycosylated soluble cleaved HIV-1 envelope trimer. Science 342(6165):1484-90.
55. Zingler K, Littman DR (1993) Truncation of the cytoplasmic domain of the simian immunodeficiency virus envelope glycoprotein increases env incorporation into particles and fusogenicity and infectivity. J Virol 67(5):2824-31.
56. Layne SP, Merges MJ, Dembo M, Spouge JL, Nara PL (1990) HIV requires multiple gp120 molecules for CD4-mediated infection. Nature 346(6281):277-9.
57. Scheid JF, Mouquet H, Feldhahn N, Seaman MS, Velinzon K, Pietzsch J, et al. (2009) Broad diversity of neutralizing antibodies isolated from memory B cells in HIV-infected individuals. Nature 458(7238):636-40.
58. Tomaras GD, Yates NL, Liu P, Qin L, Fouda GG, Chavez LL, et al. (2008) Initial B-cell responses to transmitted human immunodeficiency virus type 1: virion-binding immunoglobulin M (IgM) and IgG antibodies followed by plasma anti-gp41 antibodies with ineffective control of initial viremia. J Virol 82(24):12449-63.

59. Kunert R, Wolbank S, Stiegler G, Weik R, Katinger H (2004) Characterization of molecular features, antigen-binding, and in vitro properties of IgG and IgM variants of 4E10, an anti-HIV type 1 neutralizing monoclonal antibody. AIDS Res Hum Retroviruses 20(7):755-62.
60. Wolbank S, Kunert R, Stiegler G, Katinger H (2003) Characterization of human class-switched polymeric (immunoglobulin M [IgM] and IgA) anti-human immunodeficiency virus type 1 antibodies 2F5 and 2G12. J Virol 77(7):4095-103.
61. Munro JB, Gorman J, Ma X, Zhou Z, Arthos J, Burton DR, et al. (2014) Conformational dynamics of single HIV-1 envelope trimers on the surface of native virions. Science 346(6210):759-63.
62. Harris A, Borgnia MJ, Shi D, Bartesaghi A, He H, Pejchal R, et al. (2011) Trimeric HIV-1 glycoprotein gp140 immunogens and native HIV-1 envelope glycoproteins display the same closed and open quaternary molecular architectures. Proc Natl Acad Sci U S A 108(28):11440-5.
63. Ozorowski G, Pallesen J, de Val N, Lyumkis D, Cottrell CA, Torres JL, et al. (2017) Open and closed structures reveal allostery and pliability in the HIV-1 envelope spike. Nature 547(7663):360-3.
64. Wang H, Barnes CO, Yang Z, Nussenzweig MC, Bjorkman PJ (2018) Partially-open HIV-1 Envelope Exhibit Conformational Changes Relevant for Coreceptor Binding and Fusion. Cell Host Microbe:in press.
65. Wang H, Cohen AA, Galimidi RP, Gristick HB, Jensen GJ, Bjorkman PJ (2016) Cryo-EM structure of a CD4-bound open HIV-1 envelope trimer reveals structural rearrangements of the gp120 V1V2 loop. Proc Natl Acad Sci U S A 113(46):E7151-E8.
66. Lee JH, Andrabi R, Su CY, Yasmeen A, Julien JP, Kong L, et al. (2017) A Broadly Neutralizing Antibody Targets the Dynamic HIV Envelope Trimer Apex via a Long, Rigidified, and Anionic beta-Hairpin Structure. Immunity 46(4):690-702.
67. Kitov PI, Bundle DR (2003) On the nature of the multivalency effect: a thermodynamic model. J Am Chem Soc 125(52):16271-84.
68. Liese S, Netz RR (2015) Influence of length and flexibility of spacers on the binding affinity of divalent ligands. Beilstein J Org Chem 11:804-16.
69. Yan GH, Wang K, Shao Z, Luo L, Song ZM, Chen J, et al. (2018) Artificial antibody created by conformational reconstruction of the complementary-determining region on gold nanoparticles. Proc Natl Acad Sci U S A 115(1):E34-E43.
70. Fasting C, Schalley CA, Weber M, Seitz O, Hecht S, Koksch B, et al. (2012) Multivalency as a chemical organization and action principle. Angew Chem Int Ed Engl 51(42):10472-98.
71. Thubagere AJ, Li W, Johnson RF, Chen Z, Doroudi S, Lee YL, et al. (2017) A cargo-sorting DNA robot. Science 357(6356).
72. Varner CT, Rosen T, Martin JT, Kane RS (2015) Recent advances in engineering polyvalent biological interactions. Biomacromolecules 16(1):43-55.
73. Diskin R, Scheid JF, Marcovecchio PM, West AP, Jr., Klein F, Gao H, et al. (2011) Increasing the potency and breadth of an HIV antibody by using structure-based rational design. Science 334(6060):1289-93.
74. Zadeh JN, Steenberg CD, Bois JS, Wolfe BR, Pierce MB, Khan AR, et al. (2011) NUPACK: Analysis and design of nucleic acid systems. J Comput Chem 32(1):170-3.
75. Maes R, Sedwick W, Vaheri A (1967) Interaction between DEAE-dextran and nucleic acids. Biochemica et Biophysica ACTA (BBA) - Nucleic Acids and Protein Synthesis 134(2):269-76.
76. West AP, Jr., Scharf L, Horwitz J, Klein F, Nussenzweig MC, Bjorkman PJ (2013) Computational analysis of anti-HIV-1 antibody neutralization panel data to identify potential functional epitope residues. Proc Natl Acad Sci U S A 110(26):10598-603.
77. Berg HC (1993) Random Walks in Biology. Princeton, NJ: Princeton University Press.